

UNVEILING THE STRUCTURE OF PRE-TRANSITIONAL DISKS

C. ESPAILLAT^{1,2}, P. D’ALESSIO³, J. HERNÁNDEZ⁴, E. NAGEL⁵, K. L. LUHMAN⁶, D. M. WATSON⁷, N. CALVET⁸, J. MUZEROLLE⁹, & M. MCCLURE⁸

Draft version August 18, 2019

ABSTRACT

In the past few years, several disks with inner holes that are relatively empty of small dust grains have been detected and are known as transitional disks. Recently, *Spitzer* has identified a new class of “pre-transitional disks” with gaps based on near-infrared photometry and mid-infrared spectra; these objects have an optically thick inner disk separated from an optically thick outer disk by an optically thin disk gap. A near-infrared spectrum provided the first confirmation of a gap in the pre-transitional disk of LkCa 15 by verifying that the near-infrared excess emission in this object was due to an optically thick inner disk. Here we investigate the difference between the nature of the inner regions of transitional and pre-transitional disks using the same veiling-based technique to extract the near-infrared excess emission above the stellar photosphere. However, in this work we use detailed disk models to fit the excess continua as opposed to the simple blackbody fits used previously. We show that the near-infrared excess emission of the previously identified pre-transitional disks of LkCa 15 and UX Tau A in the Taurus cloud as well as the newly identified pre-transitional disk of Rox 44 in Ophiuchus can be fit with an inner disk wall located at the dust destruction radius. We also present detailed modeling of the broad-band spectral energy distributions of these objects, taking into account the effect of shadowing by the inner disk on the outer disk, but considering the finite size of the star, unlike other recent treatments. The near-infrared excess continua of these three pre-transitional disks, which can be explained by optically thick inner disks, are significantly different from that of the transitional disks of GM Aur, whose near-infrared excess continuum can be reproduced by emission from sub-micron-sized optically thin dust, and DM Tau, whose near-infrared spectrum is consistent with a disk hole that is relatively free of small dust. The structure of pre-transitional disks may be a sign of young planets forming in these disks and future studies of pre-transitional disks will provide constraints to aid in theoretical modeling of planet formation.

Subject headings: accretion disks, stars: circumstellar matter, planetary systems: protoplanetary disks, stars: formation, stars: pre-main sequence

1. INTRODUCTION

Several disks which have nearly photospheric near-infrared emission but substantial excesses above the stellar photosphere at wavelengths beyond $\sim 20 \mu\text{m}$ have been observed and are referred to as “transitional disks” (Strom et al. 1989). Using data from the *Spitzer* Infrared Spectrograph (IRS; Houck et al. 2004), detailed modeling has demonstrated that this flux deficit at near-infrared wavelengths relative to full disks can be ex-

plained by optically thick disks with inner holes of $< 40 \text{ AU}$. In most cases these inner holes are not completely devoid of material (e.g. GM Aur, TW Hya, CS Cha, CVSO 224); a minute amount of micron- or sub-micron-sized optically thin dust exists within the hole, producing a small infrared excess over the photospheric flux, still well below the median excess of Class II objects, as well as silicate emission (Calvet et al. 2002, 2005; Espaillat et al. 2007b, 2008b). Gas has also been detected within the inner holes of transitional disks (e.g. Najita et al. 2003; Bergin et al. 2004; Salyk et al. 2007).

Recently, the *Spitzer Space Telescope* (Werner et al. 2004) identified a new class of disks called “pre-transitional disks” around LkCa 15 and UX Tau A (Espaillat et al. 2007a). These disks have deficits of mid-infrared flux ($5\text{--}20 \mu\text{m}$) and substantial excesses at longer wavelengths, as is seen in the transitional disks. However, in contrast to the small or absent near-infrared ($2\text{--}5 \mu\text{m}$) excesses exhibited by transitional disks, pre-transitional disks have significant near-infrared excesses relative to their stellar photospheres, similar to the median spectral energy distribution (SED) of disks in Taurus (D’Alessio et al. 1999). The distinctive shapes of these SEDs indicate that pre-transitional disks have an inner disk separated from an outer disk and that we may be seeing the development of gaps within protoplanetary disks.

While the truncation of LkCa 15’s outer disk has

¹ Harvard-Smithsonian Center for Astrophysics, 60 Garden Street, MS-78, Cambridge, MA, 02138, USA; cespaillat@cfa.harvard.edu

² NSF Astronomy & Astrophysics Postdoctoral Fellow

³ Centro de Radioastronomía y Astrofísica, Universidad Nacional Autónoma de México, 58089 Morelia, Michoacán, México; p.dalessio@crya.unam.mx

⁴ Centro de Investigaciones de Astronomía (CIDA), Merida, 5101-A, Venezuela; jesush@cida.ve

⁵ Departamento de Astronomía, Universidad de Guanajuato, Guanajuato, Gto, México 36240; erick@astro.ugto.mx

⁶ Department of Astronomy and Astrophysics, The Pennsylvania State University, University Park, PA 16802, USA; kluhman@astro.psu.edu

⁷ Department of Physics and Astronomy, University of Rochester, NY 14627-0171, USA; dmw@pas.rochester.edu

⁸ Department of Astronomy, University of Michigan, 830 Denison Building, 500 Church Street, Ann Arbor, MI 48109, USA; ncalvet@umich.edu, melisma@umich.edu

⁹ Space Telescope Institute, 3700 San Martin Drive, Baltimore, MD 21218, USA; muzerol@stsci.edu

been imaged in the millimeter (Piétu et al. 2006), Espaillat et al. (2007a) showed that the substantial near-infrared excess of LkCa 15 could be explained by either optically thick material or by $\sim 10^{-11} M_{\odot}$ of optically thin dust mixed with the gas in the inner disk. In order to resolve this issue, Espaillat et al. (2008a) obtained a medium resolution near-infrared spectrum spanning the wavelength range 2–5 μm . This near-infrared spectrum had absorption lines that were weaker relative to the spectrum of a standard star of the same spectral type. This phenomenon, known as “veiling” (Hartigan et al. 1989), is also observed in similar spectra of full disks and is due to emission from dust located at the dust sublimation radius (Muzerolle et al. 2003). Espaillat et al. (2008a) measured a veiling factor (r_K) of 0.3 ± 0.2 for LkCa 15 at $\sim 2.2 \mu\text{m}$ and fit the near-infrared excess from 2–5 μm with a single-temperature blackbody of 1600 K. This behavior can be explained by an optically thick wall located at the dust sublimation radius, as is seen in full disks (Muzerolle et al. 2003). These data confirmed that LkCa 15 has an inner optically thick disk, making this observation the first independent verification of a gap in a protoplanetary disk.

Here we expand our sample to include the pre-transitional disks of UX Tau A (Espaillat et al. 2007a) and Rox 44 (Furlan et al. 2009), and the transitional disks of GM Aur and DM Tau (Calvet et al. 2005) in order to explore the structure of the inner regions of pre-transitional and transitional disks. To do this we use veiling measurements in the K-band to extract the near-infrared (-IR) excess emission of these objects and then fit this emission with disk models (D’Alessio et al. 2005; Calvet et al. 2002). Given the sensitivity of veiling measurements on the adopted spectral type, we redetermined spectral types for our targets using optical spectra (§ 4.1). We also tested our veiling measurement methods with the spectrum of the diskless, weak-line T Tauri star (WTTS) LkCa 14 (§ 4.2.1).

We find that the near-infrared spectra of the pre-transitional disks of LkCa 15, UX Tau A, and Rox 44 are well-explained by the wall of an optically thick inner disk (§ 4.2.1, § 4.2.3, § 4.2.4). In contrast, our data shows that the inner hole of the transitional disk of GM Aur contains a small amount of optically thin sub-micron-sized dust while DM Tau’s hole is relatively free of small dust (§ 4.2.5 & § 4.2.6). Our results are consistent with veiling and interferometric measurements found in the literature. We also perform detailed model fits to the broad-band SEDs of our pre-transitional disk sample, and explore the effect of shadowing of the outer disk by the inner disk (§ 4.3), taking into account that the star is not a point source, as has been adopted in other studies (Espaillat et al. 2007a; Mulders et al. 2010). The structure of pre-transitional disks suggests that of the disk clearing mechanisms proposed to date, planet formation (e.g. Goldreich & Tremaine 1980; Rice et al. 2003; Varnière et al. 2006) is most likely a dominant factor in clearing these disks.

2. OBSERVATIONS & DATA REDUCTION

Near-infrared spectra of LkCa 14, LkCa 15, UX Tau A, Rox 44, GM Aur, and DM Tau were obtained at the NASA Infrared Telescope Facility (IRTF) facility using SpEx (Rayner et al. 2003). For each of our targets, we

used the Long XD2.1 grating, covering 2.1 to 5.0 μm , with a slit of $0''.5 \times 15''$ for a resolution ($\lambda/\delta\lambda$) of 1500. To trace near-IR emission at shorter wavelengths, if present, we obtained additional spectra from ~ 0.8 –2.5 μm for LkCa 15, UX Tau A, Rox 44, and GM Aur using the low-resolution prism with a slit of $0''.8 \times 15''$ ($\lambda/\delta\lambda \sim 250$) with an exposure time of 40 seconds. The dates of the observations, the LXD exposure times, and the signal-to-noise ratios for each target are given in Table 1. We note that the prism data for Rox 44 were first presented in McClure et al. (2010).

We extracted the data with Spextool (Cushing et al. 2004) and corrected for telluric absorption using the *xtellcor* routine (Vacca et al. 2003). Our telluric standards for LkCa 14, LkCa 15, DM Tau, GM Aur, UX Tau A, and Rox 44 were HD25175, HD27777, HD27761, HD27777, HD27777, and HD146606 respectively. Bad pixels and regions of high telluric noise (e.g. 2.5–2.9 μm and 4.2–4.6 μm) were manually removed from the spectra.

To measure the spectral types for objects in our sample, we used archival low-dispersion optical spectra obtained at the 1.5 m telescope of the Whipple Observatory with the Fast Spectrograph for the Tillinghast Telescope (FAST; Fabricant et al. 1998) equipped with the Loral 512 \times 2688 CCD. The spectrograph was set up in the standard configuration used for FAST COMBO projects: a 300 groove mm^{-1} grating and a 3'' wide slit. This combination offers spectral coverage over ~ 3600 –7500 Å, with a resolution of ~ 6 Å. All spectra were reduced at the Harvard-Smithsonian Center for Astrophysics using software developed specifically for FAST COMBO observations and were wavelength-calibrated and combined using standard IRAF routines. Data for UX Tau A and LkCa 14 were obtained in 1995 and 1996 as part of Program 38 (PI: Briceño) and are publicly available in the FAST database.¹⁰ Spectra for LkCa 15, DM Tau, and GM Aur were obtained in 1995 and 1996 as part of Program 30 (PI: Kenyon) and were first used in Kenyon et al. (1998) to measure the equivalent widths of H α , [N II], He I, and [S II] lines. We note that no FAST spectra were available for Rox 44.

3. DISK MODEL

In the next section, we fit the near-IR excess emission and the broad-band SEDs of some of the objects in our sample with disk models. Below we describe the models used to reproduce the observed emission.

In the pre-transitional disks, there is an inner wall located at the dust sublimation radius which dominates the near-IR (2–5 μm) emission. Here we use the wall model of D’Alessio et al. (2005). The wall is assumed to be vertical¹¹ with evenly distributed dust. The wall’s optical depth increases radially and is optically thin closest to the star. The stellar radiation impinges directly onto the wall, with an angle of 0° to the normal of the wall’s surface. Following Calvet et al. (1991, 1992), the radial distribution of temperature for the wall atmosphere is

$$T_d(\tau_d)^4 \sim \frac{F_0}{4\sigma_R} \left[2 + \frac{\kappa_s}{\kappa_d} e^{-q\tau_d} \right] \quad (1)$$

¹⁰ <http://tdc-www.harvard.edu/cgi-bin/arc/fsearch>

¹¹ We leave it to future work to explore the curvature of the inner wall (Nagel et al. in prep).

where $F_0 = (L_* + L_{acc})/4\pi R_{wall}^2$, σ_R is the Stefan-Boltzmann constant, τ_d is the total mean optical depth in the disk, and κ_s and κ_d are the mean opacities to the incident and local radiation, respectively. L_* is the stellar luminosity and L_{acc} ($\sim GM_*\dot{M}/R_*$) is the luminosity of the accretion shock onto the stellar surface, which also heats the inner wall. To derive the location of the wall, one sets $\tau_d = 0$ and

$$R_{wall} \sim \left[\frac{(L_* + L_{acc})}{16\pi\sigma_R} \left(2 + \frac{\kappa_s}{\kappa_d} \right) \right]^{1/2} \frac{1}{T_{wall}^2}. \quad (2)$$

T_{wall} is the temperature at the surface of the optically thin wall atmosphere (i.e. $T_d(\tau_d=0)$). When fitting the wall located at the dust sublimation radius, the relevant dust grains located at these high temperatures (1000–2000 K) are composed of silicates. Following D’Alessio et al. (2005), here we adopt silicates with a dust-to-gas mass ratio (ζ_{sil}) of 0.0034 using opacities from Dorschner et al. (1995). The grain size distribution used here (and throughout the disk) follows the form $a^{-3.5}$ where a varies between a_{min} and a_{max} (Mathis et al. 1977). The temperature of the inner wall (T_{wall}^i), the height of the wall (z_{wall}^i), and the maximum grain size are adjusted to fit the SED.

In the transitional disks, there is an inner hole that sometimes contains a small amount of optically thin dust which contributes to the SED between ~ 2 – $10 \mu\text{m}$. We calculate the emission from this optically thin dust region by integrating the flux from optically thin annuli where all of the dust grains are heated by stellar radiation following Calvet et al. (2002). Some pre-transitional disks also contain optically thin dust within their disk gaps.

In both pre-transitional and transitional disks, there is an outer wall located where the outer disk is truncated and this wall dominates the SED emission from ~ 20 – $30 \mu\text{m}$. The temperature structure of this wall is calculated in the same manner as the structure of the inner wall above. For the wall of the outer disk, we add organics and troilite to the dust mixture following D’Alessio et al. (2005) with $\zeta_{org} = 0.001$ and $\zeta_{troi} = 0.000768$ and sublimation temperatures of $T_{org} = 425$ K and $T_{troi} = 680$ K. We include water ice as well where the local temperature is below the sublimation temperature of this component ($T_{ice} = 110$ K). We use $\zeta_{ice} = 0.00056$, which is 10 % of the abundance proposed by Pollack et al. (1994), since D’Alessio et al. (2006) found that Pollack et al. (1994)’s ice abundance produces features that are not observed in typical disk SEDs. Opacities for organics, troilite, and water ice are adopted from Pollack et al. (1994), Begemann et al. (1994), and Warren (1984). In this paper we do not study the detailed composition of the dust, but simply illustrate that a typical dust composition can reasonably explain the observed SED. We adopt an ISM-sized grain distribution (i.e. $a_{min} = 0.005 \mu\text{m}$ and $a_{max} = 0.25 \mu\text{m}$; Mathis et al. 1977) and varied the outer wall temperature (T_{wall}^o) and height (z_{wall}^o) to achieve the best-fit to the SED.

In the pre-transitional disks, the inner optically thick disk will cast a shadow on the outer disk. Assuming that the central star is a point source, this shadowing of the outer disk would be substantial. On the contrary, the star appears as a finite source to the outer disk and so the inner disk will cast a large penumbra and a small

umbra on the outer disk. If a point on the outer wall is in the umbra, it does not see the star. If it is in the penumbra, it will see some of the star, and will still be illuminated to some extent. If the point on the wall is completely out of the shadow (both umbra and penumbra), it is fully illuminated by the star. In calculating the outer wall’s emission we take into account shadowing by a finite source star (see Appendix). Since we assume the wall is vertical and the luminosity along the the outer wall changes due to the geometry of the shadow, there will be a range of temperatures along the surface of the wall, consistent with the varying degree of illumination. We calculate the resulting SED with this range of temperatures and the radius of the wall is determined by the temperature in the fully illuminated part.

Both pre-transitional and transitional disks have a contribution to their SEDs beyond $\sim 40 \mu\text{m}$ from the outer disk and we use the irradiated accretion disk models of D’Alessio et al. (2006) to model the emission of the disk behind the wall. To simulate grain growth and settling, the disk is composed of two dust grain size distributions. In the upper disk layers, grains are ISM-sized and in the disk midplane the maximum grain size is 1 mm (D’Alessio et al. 2006). The viscosity parameter (α) and settling parameter (ϵ ; i.e. the dust-to-gas mass ratio in the upper disk layers relative to the standard dust-to-gas mass ratio) are varied to achieve the best-fit to the SED. We adopt an outer disk radius of 300 AU for all of our disks.

4. ANALYSIS

Classical T Tauri stars tend to have observed photospheric absorption lines which are weaker than those of non-accreting stars. This “veiling” is due to an excess continuum which adds to the star’s emission and “fills in” stellar absorption lines, making them appear weaker when compared to a standard star of the same spectral type (Hartigan et al. 1989). In the optical and shorter wavelengths, this is primarily due to the hot continuum which arises from the accretion shocks onto the star (Calvet & Gullbring 1998). In the near-infrared, for stars which are not strong accretors, veiling of photospheric absorption lines is mainly due to dust in the disk (Muzerolle et al. 2003).

Since veiling measurements are dependent on the spectral types that are adopted, we first re-derive spectral types for most of our sample using FAST optical spectra in § 4.1. Then, in § 4.2 we measure near infrared veiling for our sample, extract the excess emission, and fit it with disk wall models. We then model the broad-band SEDs of the pre-transitional disks of LkCa 15, UX Tau A, and Rox 44 with the best-fit inner wall model, including the shadowing of this inner wall on the outer disk.

4.1. Spectral Type Classification

Spectral types were derived with the SPTCLASS tool,¹² an IRAF/IDL code based on the methods described by Hernández et al. (2004). The original code was optimized to calculate the spectral types of early type stars (B, A, & F) based on 33 spectral features that are sensitive to changes in T_{eff} . SPTCLASS was later

¹² <http://www.astro.lsa.umich.edu/~hernandj/SPTclass/sptclass.html>

revised to incorporate 11 spectral indices optimized for solar type stars (from middle F to early K) and 16 spectral indices optimized for low mass stars (from early K to M5). Each spectral index is obtained by measuring the decrease in flux from what would be expected at the line center by interpolating between two adjacent bands on each side of the line. Each index is calibrated using spectroscopic standards observed with FAST.

Most of the spectral classifications derived in this work differ somewhat from those reported in the literature. Our classification of DM Tau ($M1.5 \pm 1.0$) is in agreement with previous measurements of M0.5 (Cohen & Kuhi 1979) and M2 (Herbig 1977). However, we measure a spectral type for LkCa 14 of $K5.5 \pm 1.0$ while Herbig et al. (1986) derived a spectral type of M0. For GM Aur, we derive a spectral type of $K5.5 \pm 1.0$, but in the literature we find spectral classifications of K3 (Herbig 1977) and K7–M0 (Cohen & Kuhi 1979) for this object. We derive a spectral type of $K3 \pm 1.0$ for LkCa 15 which differs from the K5 spectral type for this object reported by Herbig et al. (1986). We classify UX Tau A as a $G8.0 \pm 2.0$ star; Herbig (1977) and Cohen & Kuhi (1979) both reported a spectral type of K2, Rydgren et al. (1976) reported G5, and Hartigan et al. (1994) find K5–K2. Since no FAST spectra are available for Rox 44, we adopt a spectral type of K3 from Bouvier & Appenzeller (1992) for this object.

The spectral types derived here (Table 2) are based on a greater number of spectral indices than used in the works cited above. Since commonly used spectral indices such as He I (4922 Å, 5016 Å) and Na I (5890 Å, 5896 Å) can be affected by emission or anomalous absorption, it is crucial to base spectral type measurements on several indices (see discussion in Hernández et al. 2004). Herbig (1977), Herbig et al. (1986), Rydgren et al. (1976), and Cohen & Kuhi (1979) analyze spectral ranges of 5850–6700 Å, 5800–6800 Å, 3500–7000 Å, and 4270–6710 Å, respectively, with a resolution similar to that of our observations, but with fewer spectral indices. The medium resolution (~ 2 Å) spectra by Hartigan et al. (1994) cover a much smaller range in wavelength (5700–6900 Å and 5860–6890 Å) that includes few spectral indices. We include more indices and these are based on a library of standards obtained with the same instrument and configuration.

In Figures 1, 2, and 3 we illustrate the accuracy of the SPTCLASS fitting procedure by comparing our targets to spectral type standards. In the late-type stars, the molecular bands of TiO and CaH were used in classifying the targets (Figures 1 and 2). In G-type stars, the metallic lines play an important role in spectral classification and the features used to classify UX Tau A include the Ca I, Mg I, Fe I, and Ca I lines (Figure 3). The TiO and CaH bands in LkCa 14 (Figure 2) are in better agreement with a K5/K6 star. In GM Aur and LkCa 15, these bands are similar to those in a K5/K6 star and K4/K3 star, respectively, rather than earlier (Figure 2) or later (Figure 1) type stars. The lines in UX Tau A, particularly Ca I and Na I, are weaker than those in a later type star (e.g. K1) and resemble the depths of the lines in the G8 star but not the earlier type stars (Figure 3). Since there are no G6 or G7 objects in the library of standards used for our classification we cannot exclude it is a G6 or

G7 star and so the uncertainty in UX Tau A’s G8 spectral type classification is ± 2.0 . We note that our SpeX spectra are consistent with the spectral types derived with FAST.

4.2. Near-Infrared Excess Emission

To estimate the amount of veiling present in our sample, we compared the line strengths in the target to those of a standard star of the same spectral type (§ 4.2). The spectra of corresponding template stars were obtained from the IRTF Spectral Library (Cushing et al. 2005; Rayner et al. 2009)¹³. We first normalized the target and standard stars’ emission at $2.2 \mu\text{m}$ and then artificially veiled the standard spectrum by adding a flat continuum of $F_{\text{excess}} = r_K \times F_{\text{standard}}$ where r_K is the veiling factor ($= F_{\text{excess}}/F_*$). The standard spectrum was veiled until the depths of the absorption lines matched those of the target spectrum between $2.20 - 2.28 \mu\text{m}$. We normalized the standard spectrum in the K-band to the colors of a corresponding stellar photosphere from Kenyon & Hartmann (1995) scaled to the observed J-band flux. We then scaled the target by $1 + r_K$ and subtracted the standard spectrum to extract the shape of near-infrared excess emission. When excess emission is present, we fit the continuum with a disk model and derive the best-fit parameters.

4.2.1. LkCa 14

To test our method of measuring the veiling and excess emission of T Tauri stars (TTS), we analyzed the spectrum of LkCa 14, a single (White & Ghez 2001), non-accreting diskless T Tauri star in Taurus (Kenyon & Hartmann 1995). The expectation is that this object should have no K-band veiling since it does not exhibit excess emission at near- and mid-IR wavelengths in its SED (Kenyon & Hartmann 1995). Karr et al. (2010) report a tentative detection of dust around LkCa 14 based on H-band scattered light images, however, LkCa 14’s emission is photospheric out to $\sim 24 \mu\text{m}$ (Luhman et al. 2010), making it suitable for the purposes of this work.

We measure the amount of veiling in LkCa 14 by comparing its K-band spectrum to that of a K5 V spectral standard from the IRTF spectral library (HD36003). We find that LkCa 14 has no veiling ($r_K = 0 \pm 0.2$) from $2.20 - 2.28 \mu\text{m}$. In order to extract any excess emission between $2 - 5 \mu\text{m}$, if present, we first deredden the spectra. The standards from the IRTF library have already been corrected for reddening. For LkCa 14, we measure a visual extinction (A_V) of 0 by matching V (Høg et al. 2000), R (Norton et al. 2007), and 2MASS photometry to the colors of a K5 stellar photosphere (Kenyon & Hartmann 1995) which is scaled to the J-band photometry. We subtract the standard from the target and find that there is no significant excess emission at longer wavelengths (Figure 4). There is a small mismatch between the two spectra from $\sim 3.5 - 4.2 \mu\text{m}$ which is most likely due to uncertainties in the measured spectral slopes of the target.

We conclude that, as expected, LkCa 14 has no veiling and no excess emission. This indicates that for the purposes of this work dwarfs in the IRTF online library are suitable templates.

¹³ http://irtfweb.ifa.hawaii.edu/~spex/IRTF_Spectral_Library/

4.2.2. LkCa 15

Espaillet et al. (2008a) measured a veiling factor at $\sim 2.2 \mu\text{m}$ of 0.3 ± 0.2 for LkCa 15. Using this veiling factor, they extracted the excess emission spectrum from the SpeX data and fit it with a simple blackbody at a temperature of 1600 K, corresponding to the behavior expected from the wall of an inner optically thick disk. This blackbody fit, when taken in conjunction with the dust clearing inferred from the broadband SED (Espaillet et al. 2007a) and millimeter imaging (Piétu et al. 2006), made LkCa 15 the first confirmed gapped disk around a TTS.

Here we present new SpeX data from $\sim 0.8\text{--}5 \mu\text{m}$ for LkCa 15 and analyze the near-IR excess emission of this object in more detail by fitting it with the disk wall model of D’Alessio et al. (2005). We compare LkCa 15 a K3 V spectral standard (HD219134) from the IRTF library and measure an r_K of 0.6 ± 0.2 . While this is in agreement with Espaillet et al. (2008a) within the uncertainties, it may also reflect infrared variability as has been observed in transitional disks (Muzerolle et al. 2009). We scaled the spectrum of LkCa 15 relative to the template according to this veiling factor and dereddened the LkCa 15 spectrum using the Mathis (1990) dereddening law until it agreed with the template spectrum at $1 \mu\text{m}$. In this manner, we measure an extinction of 1.3. Extinction measurements based on matching V-, R-, I-band, and 2MASS photometry to photospheric colors from Kenyon & Hartmann (1995) derive $A_V = 1.7$. If we scale LkCa 15’s spectrum using $r_K = 0.4$, which is within the veiling measurement uncertainty, we measure a visual extinction of 1.3 and so the difference in A_V is within the uncertainties of the veiling determination. Alternatively, this may be a reflection of the fact that in some cases one can derive higher visual extinctions using color indices at longer wavelengths than V-R (Gullbring et al. 1998).

After subtracting the template spectrum from the target spectrum to extract the excess above the stellar photosphere, we fit the residual excess continuum with a disk wall model (Figure 5). For the inner wall model of LkCa 15, we adopt the stellar properties listed in Table 3 which were obtained with the Siess et al. (2000) evolutionary tracks. The mass accretion rate of LkCa 15 was estimated from its U-band excess following Gullbring et al. (1998). We adopt a minimum grain size of $0.005 \mu\text{m}$ as is typically assumed for the interstellar medium (Mathis et al. 1977) and vary the maximum grain size and the temperature of the optically thin wall atmosphere (T_{wall}^i) to achieve the best-fit to the SpeX excess emission. We test wall temperatures between 1000–2000 K, corresponding to the range of dust sublimation temperatures found for a large sample of classical T Tauri stars (CTTS) and Herbig Ae/Be stars (Monnier & Millan-Gabet 2002), and maximum grain sizes of $0.25 \mu\text{m}$, $1 \mu\text{m}$, and $5 \mu\text{m}$. LkCa 15 has significant $10 \mu\text{m}$ silicate emission, indicative of small grains, and therefore we do not test larger grain sizes. The best-fit wall to the excess emission has a temperature of 1400 K, a height of 0.017 AU, and a maximum grain size of $1 \mu\text{m}$ which, according to Eq. 2, corresponds to a wall located ~ 0.12 AU from the central star (Figure 5). This detailed model fit is consistent with the simple 1600 K blackbody fit found in earlier work (Espaillet et al. 2008a). The

difference in temperature follows from the additional parameters included in the wall model, namely the effect of the dust properties and the inclusion of an optically thin wall atmosphere. Our detailed fit to the excess continuum is consistent a veiling measurement at $\sim 4.8 \mu\text{m}$ by Salyk et al. (2009) (see Figure 5).

4.2.3. UX Tau A

UX Tau A was first modeled as a pre-transitional disk by Espaillet et al. (2007a). To discern the nature of the innermost disk of this object, here we compare UX Tau A to a standard star of G8 V (HD101501) from the IRTF library and find that the absorption lines in the K-band spectrum of UX Tau A are weaker than those in the spectrum of the standard dwarf between $2.20\text{--}2.28 \mu\text{m}$. We measure an r_K of 0.4 ± 0.2 which is consistent with 2MASS K-band photometry, from which we infer an r_K of 0.3.

We scale UX Tau A’s SpeX spectrum relative to the template according to the derived veiling factor and deredden the target spectrum until it agrees with the template spectrum at $1 \mu\text{m}$. We measure an extinction of 2.3 using this method, however, we derive an A_V of 1.8 for UX Tau A by comparing V-, R-, I-band (Kenyon & Hartmann 1995) and 2MASS photometry to a standard G8 photosphere’s colors (Kenyon & Hartmann 1995). This difference in A_V is within the uncertainties of the veiling determination.

After extracting the near-infrared excess of UX Tau A (Figure 5), we fit it with the wall model described in § 3. We use the stellar parameters (M_* , R_* , L_*) listed in Table 3 which were derived from the HR diagram and the Siess et al. (2000) evolutionary tracks, and we adopt an inclination for UX Tau A of 60° . As with LkCa 15, we adopt a minimum grain size of $0.005 \mu\text{m}$ and vary the temperature of the wall between 1000–2000 K. Since there is no $10 \mu\text{m}$ silicate feature in UX Tau A, indicating a lack of small grains, we adopt a maximum grain size of $10 \mu\text{m}$. We cannot discriminate between wall fits using a maximum grain size of $10 \mu\text{m}$, $100 \mu\text{m}$, or $1000 \mu\text{m}$, however, since the wall’s parameters (z_{wall}^o , R_{wall}^o) do not vary significantly between the three grain sizes for the purposes of this work, we adopt the smallest maximum grain size that can reproduce the SpeX excess spectrum. We find that the best-fit wall has a surface temperature of ~ 1550 K, is located 0.15 AU from the star, and has a height of 0.009 AU (Figure 5). Our results are consistent with other veiling measurements found in the literature. Edwards et al. (2006) measure a veiling of 0 at $1 \mu\text{m}$ and Salyk et al. (2009)’s veiling measurement at $\sim 4.8 \mu\text{m}$ is consistent with our analysis within the veiling measurement uncertainties (see Figure 5).

4.2.4. Rox 44

Rox 44, located in the Ophiuchus cloud, was identified as a pre-transitional disk candidate based on its strong $10 \mu\text{m}$ silicate emission feature which could not be explained by full disk models (Furlan et al. 2009; McClure et al. 2010). Rox 44’s *Spitzer* IRS spectrum is also strikingly similar in shape to that of LkCa 15. To investigate the nature of the inner disk of Rox 44, we obtained a near-IR SpeX spectrum. When compared to a K3 V standard (HD219134) from the IRTF library, the absorption lines in the K-band spectrum of Rox 44 are weaker between

2.20 – 2.28 μm and we measure an r_K of 0.8 ± 0.2 , consistent with an r_K of 0.7 inferred from 2MASS K-band photometry.

We scale the spectrum of Rox 44 relative to the template according to this veiling factor and deredden its spectrum until it agrees with that of the template spectrum at 1 μm (Figure 5). We measure a visual extinction of 2.2, in agreement with previous extinction measurements from Bouvier & Appenzeller (1992).¹⁴ The excess emission above the stellar photosphere can be fit with a wall model (Figure 5) using the stellar parameters in Table 3 and adopting a minimum grain size of 0.005 μm . We tested maximum grain sizes of 0.25 μm , 1 μm , and 5 μm and temperatures between 1000–2000 K. The best-fit wall to the near-infrared excess continuum of Rox 44 has a height of 0.034 AU, a maximum grain size of 1 μm , a temperature of 1200 K, and is located 0.25 AU from the central star (Figure 5).

4.2.5. GM Aur

We now turn to the transitional objects in our sample. The transitional disk around the single star GM Aur (Pott et al. 2010; White & Ghez 2001, A. Kraus, private communication) has an inner hole of ~ 20 AU (Hughes et al. 2009) which contains some sub-micron-sized optically thin dust (Calvet et al. 2005). In our veiling analysis, we compare GM Aur to a K5V standard (HD36003) and find that GM Aur’s K-band absorption lines are slightly veiled ($r_K=0.1 \pm 0.2$) and the object exhibits a small excess above the stellar photosphere (Figure 5). This veiling measurement is consistent with a veiling factor of 0.2 inferred from 2MASS K-band photometry.

After scaling the GM Aur spectrum according to its veiling factor, we derive an extinction (A_V) of 1.2 by dereddening its spectrum with the Mathis (1990) law until it matches the template spectrum at 1 μm . However, as in the case of LkCa 15 and UX Tau A, this is higher than the extinction of 0.8 measured by matching V, R, and I photometry (Kenyon & Hartmann 1995), and 2MASS fluxes to photospheric colors from Kenyon & Hartmann (1995).

The small excess seen in GM Aur’s SpeX spectrum is in line with the excess emission above the photosphere seen in its SED from ~ 3 –8 μm (Calvet et al. 2005). Calvet et al. (2005) showed that this emission comes from optically thin sub-micron-sized dust located within the inner 5 AU of GM Aur’s 20 AU hole. We can fit the SpeX excess of GM Aur with an optically thin dust model (Figure 5) supporting the conclusions of Calvet et al. (2005). The optically thin dust region lies within ~ 1 AU of the star and is composed of $\sim 2 \times 10^{-12} M_\odot$ of dust made up of silicates (47%), organics (42%), and troilite (11%). The total emission of this optically thin region is scaled to the vertical optical depth at 10 μm ($\tau_0 \sim 0.021$). We note that since the structure of the dust within the holes of transitional disks is not known at this time, our results should be taken as an approximation of how much

dust is needed within the hole to reproduce the SED, not as a detailed fit from which we can derive the spatial distribution of the optically thin dust near the star. High-resolution near-IR interferometry is needed to trace this component in more detail.

Our results are in agreement with other veiling measurements at 1 μm (Edwards et al. 2006) and 2.2 μm (Folha & Emerson 1999). We note that the excess emission of GM Aur derived here does not agree with the J-band veiling measurement of Folha & Emerson (1999). However, these authors use a later spectral type standard (K7) in their analysis which could have resulted in the higher veiling measurement since later type stars have deeper absorption lines. Alternatively, this may be a result of variability as is seen in other transitional disks (Muzerolle et al. 2009).

4.2.6. DM Tau

DM Tau is a single star (Pott et al. 2010; White & Ghez 2001, A. Kraus, private communication) surrounded by a transitional disk with a ~ 3 AU hole that is empty of small dust grains (Calvet et al. 2005). The absorption lines of DM Tau are not veiled relative to a M1 V standard (HD42581; Figure 6) and we measure an r_K of 0 ± 0.2 between 2.20 – 2.28 μm in the SpeX spectrum.

We derive an extinction of (A_V) of 0.7 for DM Tau by fitting V-, R-, I-band photometry (Kenyon & Hartmann 1995) and 2MASS colors to an M1 stellar photosphere from Kenyon & Hartmann (1995). The spectrum is dereddened with this extinction and the Mathis (1990) dereddening law. We note that we did not obtain a low-resolution SpeX spectrum at shorter wavelengths for this target. Subtraction of the standard from the target reveals that DM Tau exhibits no significant near-IR excess emission at 2–5 μm (Figure 6), in agreement with its lack of emission above the photosphere in the K-band (see SED in Calvet et al. 2005 or Furlan et al. 2006) as well as a veiling measurement at ~ 4.8 μm that is consistent with no excess emission at this wavelength (Salyk et al. 2009). As in the case of LkCa 14, DM Tau shows a small mismatch when compared to the standard, which may be an indication of spectral slope uncertainties. The lack of veiling and near-IR excess emission in DM Tau is consistent with the fact that this object has no excess emission above the photosphere from the K-band up to ~ 8 μm (Calvet et al. 2005), indicating that DM Tau has relatively no small dust within its hole.

4.3. Broad-Band SED Modeling of Pre-Transitional Disks

Here we model the broad-band SEDs of the pre-transitional disks of LkCa 15, UX Tau A, and Rox 44 with the best-fit inner wall model from § 4.2, including the shadowing of this inner wall on the outer disk. LkCa 15 and UX Tau A have been modeled previously (Espaillat et al. 2007a), but here we incorporate their newly derived stellar properties (§ 4.1), and inner walls (§ 4.2.2 and § 4.2.3), and a finite star.

4.3.1. LkCa 15

For LkCa 15, we measure a 58 AU gap that contains some small optically thin dust. This is compatible with

¹⁴ This extinction differs from the $A_V=3.3$ reported by McClure et al. (2010) based on near-IR colors. In this work we adopt an A_V that agrees with the optical photometry. More optical photometry is needed to better determine the extinction of this object.

millimeter interferometric imaging by Piétu et al. (2006) which finds a cavity of 46 AU in this disk, especially when one takes into account the uncertainties introduced by dust opacity one assumes (see § 5.2). Figure 7 contains the broad-band SED of LkCa 15. Observations include ground-based optical photometry (open circles; Kenyon & Hartmann 1995), and J, H, K (filled circles; 2MASS), SpeX (red solid line; this work), *Spitzer* IRAC (blue solid triangles; Luhman et al. 2010), *Spitzer* IRS (blue solid line; Furlan et al. 2006), IRAS (open triangles; Weaver & Jones 1992), and millimeter (filled pentagon from Andrews & Williams 2005; open pentagons from Espaillat et al. 2007) data. The SpeX spectrum used in this paper is not flux calibrated; here we scale it to the adopted stellar photosphere (Kenyon & Hartmann 1995) using the veiling derived in § 4.2.2

In Figure 7, we use the best-fit wall model found in § 4.2.2. We note that while this wall is a good fit to the SpeX spectrum, it over-predicts the *Spitzer* IRAC and IRS data. This can be explained by the uncertainties inherent in our veiling measurement or the fact that infrared variability in these types of disks is common (Espaillat et al., in preparation; Muzerolle et al. 2009). The 10 μm silicate emission can be fit by an optically thin dust model which contains $\sim 2 \times 10^{-11} M_{\odot}$ of optically thin dust within the inner 4 AU of the gap. This region is composed of 79% silicates, 12% organics, and 9% troilite and the total emission is scaled to the vertical optical depth at 10 μm ($\tau_0 \sim 0.009$). The outer disk has $\alpha=0.0005$ and $\epsilon=0.001$ and is inwardly truncated at about 58 AU. The inner wall dominates the near-IR emission and we constrain the inner disk to $<.19$ AU in radius, assuming that the inner disk has the same α and ϵ as the outer disk. Model parameters are listed in Table 3.

Our results for LkCa 15 differ from Espaillat et al. (2007a). In first modeling the outer disk of LkCa 15, Espaillat et al. (2007a) adopted a spectral type of K5 ($T_*=4350$ K) for this object following Herbig et al. (1986). However, the spectral type we derived in § 4.1 for LkCa 15 (K3) corresponds to a higher temperature ($T_*=4730$ K) than previously adopted. The largest difference between the disk model presented here and that in Espaillat et al. (2007a) is the location of the outer disk wall. Assuming a spectral type of K5 the disk wall was located at 46 AU while for a K3 star the wall is located at 58 AU. This difference is expected since the location of the wall, given by Eq. 2, depends on L_* and L_{acc} and these parameters are now higher with respect to the previous model.

Based on the equations presented in the Appendix, the inner wall of LkCa 15 would cast an umbra of about 7 AU on the outer wall (measured from the midplane) in the case that the star is taken to be a point source. If the star is taken to be a finite source, LkCa 15's outer wall has an umbra of ~ 4 AU and the upper edge of the penumbra is located at ~ 9 AU (Eq. A4 & A5). The result for the solid angle (Eq. A6) of the star seen by an observer at different heights of the outer wall of LkCa 15 is shown in Figure 8. Taking into account the shadowing of a finite star, the outer wall of LkCa 15 is 12.9 AU high. This is 2.6 H , where H is the gas scale height, and is consistent within 15% of the independently calculated height of the outer disk (11.7 AU) at ~ 58 AU. Therefore, while the outer wall is partially shadowed by the inner wall, we

conclude that the outer disk behind the wall is not completely shadowed by the inner disk. The height of outer wall in this work is higher than previously reported by Espaillat et al. (2007a). The z_{wall} in that paper represents the part of the wall that is illuminated when the star is taken to be a point source, but was mistakenly defined as the height of the wall above the midplane.

4.3.2. UX Tau A

For UX Tau A, we find a 71 AU gap that is relatively devoid of small dust grains, as indicated by its lack of a 10 μm silicate feature (Figure 9). Observations shown in Figure 9 include ground-based optical photometry (open circles; Kenyon & Hartmann 1995), J, H, K photometry (filled circles; 2MASS), a SpeX spectrum (solid red line; this work), *Spitzer* IRAC photometry (blue solid triangles; Luhman et al. 2010), a *Spitzer* IRS spectrum (blue solid line; Furlan et al. 2006), IRAS photometry (open triangles; Weaver & Jones 1992), and millimeter data (pentagons; Andrews & Williams 2005). Our SpeX spectrum is not flux-calibrated and we scale it to the adopted stellar photosphere using the veiling derived in § 4.2.3.

We use the best-fit wall model found in § 4.2.3 in fitting the SED emission presented in Figure 9. We find that the outer disk has $\alpha=0.004$ and $\epsilon=0.001$ and is inwardly truncated at about 71 AU. The inner wall dominates the near-IR emission and we constrain the inner disk, assuming it has the same settling and viscosity as the outer disk, to $<.21$ AU in radius. Model parameters are listed in Table 3.

The outer wall of UX Tau A would have an umbra of about 4 AU in the case that the star is taken to be a point source. If the star is taken to be a finite source, the size of the umbra is ~ 0.4 AU and the upper limit of the penumbra is ~ 8 AU. The result for the solid angle seen by an observer at different heights of the outer wall of UX Tau A is shown in Figure 8. The outer wall of UX Tau A is 13.8 AU (2.0 H) high and is consistent within 15% of the height of the outer disk (12.5 AU) at ~ 71 AU, which is calculated independently. The fully illuminated part of the outer wall is at a temperature where ice has sublimated (110 K), however, in the partially shadowed portions of the wall the temperature is lower. In order to make the composition of the wall consistent, we remove ice from the partially shadowed portions of the wall. We note that UX Tau A has crystalline silicates (Espaillat et al. 2007a), which we do not include here and would contribute to the IRS spectrum between $\sim 20 - 35 \mu\text{m}$.

As in the case of LkCa 15, our results for UX Tau A differ from Espaillat et al. (2007a) because we are adopting a different spectral type in this paper. Espaillat et al. (2007a)'s model was based on a spectral type of K2 ($T_*=4900$ K) following Herbig (1977) and Cohen & Kuhn (1979). The spectral type we derived in § 4.1 for UX Tau A (G8) corresponds to a significantly higher temperature ($T_*=5520$ K) than previously adopted. The difference in R_{wall}^o is expected following Eq. 2.

4.3.3. Rox 44

Rox 44 has a 36 AU gap that contains some ISM-sized optically thin dust. The size of this gap is consistent with the 33 AU cavity observed with the *SMA*

(Andrews et al. 2009). Observations shown in Figure 10 include ground-based optical (open circles; Herbst et al. 1994), J, H, K (filled circles; 2MASS), SpeX (solid red line; this work), *Spitzer* IRAC and MIPS (Evans et al. 2009; Padgett et al. 2008, blue solid triangles), *Spitzer* IRS (blue solid line; Furlan et al. 2006), and millimeter (pentagons; Andrews et al. 2009; Nuernberger et al. 1998) data. The SpeX spectrum is scaled to the adopted stellar photosphere using the veiling derived in § 4.2.4.

We use the best-fit wall model found in § 4.2.4 in the SED model fit presented in Figure 10. Rox 44 has $\sim 2 \times 10^{-11} M_{\odot}$ of optically thin dust within 2 AU that contributes to the 10 μm silicate feature and that is composed of 79% silicates, 12% organics, and 9% troilite. The total emission of this region is scaled to the vertical optical depth at 10 μm , $\tau_0 \sim 0.036$. The outer disk has $\alpha=0.006$ and $\epsilon=0.01$ and is inwardly truncated at about 36 AU. The inner wall dominates the near-IR emission and we constrain the inner disk to $< .4$ AU in radius. Model parameters are listed in Table 3.

In the case that the star is taken to be a point source, the outer wall of Rox 44 would have an umbra of ~ 5 AU. For a finite-source star, the size of the umbra is ~ 4 AU and the upper edge of the penumbra is located at ~ 6 AU (see Figure 8). Taking into consideration this shadowing of the outer disk, the outer wall of Rox 44 has $z_{\text{wall}}^o=9.9$ AU (3.5 H) and this height is consistent within $\sim 35\%$ with the height of the outer disk at ~ 36 AU (7.3 AU). We note that far-infrared variability is likely in this object given that the *Spitzer* IRS and MIPS data were taken at different epochs and are not in agreement, even when taking the uncertainties of the observations into consideration. If the far-infrared flux of Rox 44 was less than is seen in Figure 10 at the time when the SpeX observations were taken, then we would be overestimating the height of the outer wall. Simultaneous observations of this object in the near- and far-infrared would be useful in testing this. Additional far-infrared and sub-millimeter data would also help further constrain the properties of the outer disk.

5. DISCUSSION

5.1. Pre-Transitional Disk Structure

It is now accepted that full disks have a sharp transition at the dust destruction radius, inside of which the temperature is too high for dust to exist. This transition appears as a “wall” that is frontally illuminated by the star, since for typical mass accretion rates the inner disk gas is optically thin (Muzerolle et al. 2004). Muzerolle et al. (2003) found that nine T Tauri stars surrounded by full disks in Taurus had SpeX near-IR excess emission which could be fit by single temperature blackbodies with temperatures that fell within the range of dust sublimation temperatures (1000–2000 K) found for a larger sample by Monnier & Millan-Gabet (2002). Muzerolle et al. (2003)’s fits are evidence that there is optically thick material located at the dust destruction radius in these full disks, most likely from the inner wall of the disk which emits primarily in the near-IR.

Pre-transitional disks exhibit the same behavior as full disks in the near-IR. In this work, we can fit the continua between 1–5 μm of the pre-transitional disks in our sample with an inner disk wall which is located at the dust

destruction temperature. This conclusion is consistent with independent veiling measurements found in the literature (see § 4.2) as well as near-IR interferometric measurements. Using the Keck interferometer, Pott et al. (2010) find that the K-band emission of LkCa 15 and UX Tau A originates from very small radii. This is in good agreement with what we report in this work (Table 3) if one takes into account that Pott et al. (2010) used simple models assuming a face-on disk and the derived radii depend on the dust opacities that are adopted. Independent SED modeling also supports that the inner disk of LkCa 15 is optically thick (Mulders et al. 2010). We note that Mulders et al. (2010) claim that the optically thick inner disk of LkCa 15 extends out to 1 AU based on fitting broad-band photometry and assuming that the shadowing in the disk is due to a point source. This radius is inconsistent with the results of Pott et al. (2010) and we find that an inner disk of this size does not fit the *Spitzer* IRS spectrum.

While pre-transitional disks have the same behavior as full disks in the near-IR, at longer wavelengths in their SEDs and in millimeter images, they display evidence for large dust clearings within the disk. In the *Spitzer* IRS spectra of LkCa 15, UX Tau A, and Rox 44, we see a pronounced decrease in the emission at $\sim 20 \mu\text{m}$ which indicates a drop in the opacity of the disk, most likely due to the removal of dust. This is supported by millimeter interferometric observations of LkCa 15 (Piétu et al. 2006), UX Tau A (S. Andrews, private communication), and Rox 44 (Andrews et al. 2009) which see cavities in the images and sharp drops in the visibilities, evidence that dust in the disk has been removed. In conjunction with the evidence for an optically thick inner disk, this leads one to the conclusion that pre-transitional disks have gaps in their disks.

These gaps in pre-transitional disks are clearly different from the inner holes detected in transitional disks (see Figure 11 for a schematic). DM Tau has an inner hole of 3 AU which is relatively clear of small dust as indicated by the lack of near-infrared emission in its *Spitzer* IRS spectrum (Calvet et al. 2005). This is supported by the lack of veiling in the K-band as well as photospheric near-infrared emission, resembling what is seen in the diskless LkCa 14, indicating that the inner disk of DM Tau is devoid of small dust. GM Aur is another transitional disk studied in this paper and its SED indicates that it has a ~ 20 AU hole (Calvet et al. 2005) which has been confirmed in the millimeter (Hughes et al. 2009). GM Aur has a small excess above the photosphere in the near-infrared, as measured by its *Spitzer* IRS spectrum, which has been interpreted as originating from optically thin dust located within the disk hole (Calvet et al. 2005). In this work we demonstrate that the small, flat near-IR excess continuum extracted from the SpeX spectrum can be fit by a model with $\sim 10^{-12} M_{\odot}$ of optically thin dust within 1 AU of the star. About 85% of the emission in the K-band originates in the inner 0.5 AU of the disk, consistent with near-interferometric measurements (Pott et al. 2010).

An alternative model for the inner disk of pre-transitional disks proposed by Espaillat et al. (2007a) and further investigated by Mulders et al. (2010) is that the inner disks of these objects are optically thin. However, GM Aur’s near-IR emission is strikingly differ-

ent from that seen in our pre-transitional disk sample. GM Aur’s near-IR excess is relatively flat, reflecting a range of different temperatures. On the other hand, the near-IR excess emission of pre-transitional disks resembles a single temperature blackbody. Optically thin dust spread out over several radii will not appear as a single temperature blackbody and if one confines this optically thin dust to very small radii, one would need a shell of dust engulfing the star (Mulders et al. 2010) for which there is yet no supporting evidence.

Since the inner disk in pre-transitional disks is optically thick, it will cast a shadow on the outer disk. The shadow cast by the inner wall on the outer wall has significant consequences on the sizes of gaps that we can detect with *Spitzer*. The majority of the emission traced by IRS comes from within the inner 10 AU of the disk and over 80% of the emission at 10 μm comes from within 1 AU (D’Alessio et al. 2006; Espaillat 2009). Therefore, the *Spitzer* IRS instrument will be most sensitive to clearings in which some of the dust located at radii <1 AU has been removed. To test the limits of the smallest gap IRS could detect around a K-type star, we simulated gaps in a disk around a 0.5 M_{\odot} star with a mass accretion rate of $10^{-8} M_{\odot} \text{ yr}^{-1}$, an ϵ of 0.01, and an inclination of 60° . In this disk, we find that the smallest gap that will cause a noticeable “dip” in the *Spitzer* spectrum will be ~ 4 AU. As is seen in Figure 12, the SED of such a gapped disk begins to differ from that of a full disk beyond 10 μm . This is because, relative to a full disk, there is extra emission from the wall of the outer disk. Since the height of the disk increases with radius, the inner disk can only extend from the dust destruction radius (0.12 AU) out to about 0.3 AU before it significantly shadows the outer wall, thereby dimming the emission of the outer wall and making it indistinguishable from a full disk. Furthermore, IRS cannot easily detect gaps whose inner boundary is outside of 1 AU (e.g. a gap spanning 5–10 AU in the disk; Espaillat 2009) and it will be up to *ALMA* to detect such gaps.

There are some caveats to keep in mind regarding the above estimate of the IRS gap detection limit. First, we are assuming that the inner disk has the same amount of dust settling as the outer disk. However, if the inner disk is more settled it will have a lower surface and will not obscure the outer wall as much, and so the inner disk could extend out to further radii. Also, our simulations do not include optically thin dust within the gap and we note that we did not include any possible shadowing of dust in the optically thin regions inside the gaps of LkCa 15 and Rox 44. Infrared interferometry is crucial to explore how the spatial distribution of this component is shaped as it filters into the gap from the outer disk (Rice et al. 2006) or how it is influenced by possible planets in the gap (Lubow & D’Angelo 2006).

5.2. Dust Opacities

The opacity of the disk is controlled by dust and in any sophisticated disk model the largest uncertainty lies in the adopted dust opacities. The dust opacity sets the location of the disk surface, i.e. where the optical depth to the stellar radiation reaches ~ 1 , and in turn the amount of disk flaring. The shape of the disk surface dictates the fraction of the stellar radiation that is captured by the disk, and as a result, the heating of the disk and the

ensuing disk emission (Calvet et al. 1991).

The SED models derived in this work are obviously tied to the dust opacity that is assumed in § 3. In particular, R_{wall}^o depends on the adopted opacity following Eq. 2. We find that by adopting the dust opacities of Draine & Lee (1984), the derived R_{wall}^o of our targets increases by ~ 10 AU. This occurs because the opacity to the stellar radiation (κ_s), which peaks around 1 μm , is higher for the dust composition of Draine & Lee (1984) than that adopted in this work (Figure 13). For Pollack et al. (1994)’s opacities, R_{wall}^o decreases by ~ 10 AU. In this case, the opacity to the disk’s local emission (κ_d), which peaks $\sim 25 \mu\text{m}$, is much higher than ours.

The major differences between the opacities we adopt here and those of Draine & Lee (1984) and Pollack et al. (1994) are the assumed carbon component and the ice abundance. While most models assume some carbon component in their dust composition, there is yet no general consensus on the species of the carbon grains. Draine & Lee (1984) assume that the carbon component is due to graphite and Pollack et al. (1994) assume it is due to organics. Further study is needed to better determine the carbon component in accretion disks. The *Herschel* mission is an excellent opportunity to learn more about water ice in disks. Pollack et al. (1994) adopt a dust-to-gas mass ratio for water ice of 0.0056 while D’Alessio et al. (2006) find that the features produced by this value do not agree with observations of disks. *Herschel* can help settle this issue by detecting water lines in the far-infrared and allowing derivations of the abundance of water in disks.

5.3. Implications of Pre-Transitional Disks on Dust Clearing Mechanisms

Several mechanisms have been proposed to explain disk clearing. These include planets, grain growth, the magnetorotational instability, and photoevaporation by the central star. The structure of pre-transitional disks - an inner disk, a gap, and an outer disk - is predicted by planet formation models. On the other hand, the three alternative clearing mechanisms struggle to make a gapped disk structure and, due to their predominantly inside-out clearing pattern, are instead more likely to form a central hole in a disk.

Given the simple stipulation of a disk gap, planets emerge as the most likely dust clearing mechanism in pre-transitional disks. To further explore this possibility, one must ascertain if planet formation timescales are in line with the ages of these disks, if there is enough mass in these disks to have formed planets, and if planets can open the kind of gaps that we are detecting. Assuming that planets are indeed present within these disk gaps, one can attempt to place some constraints on theoretical planet formation models.

It is feasible to form planets within 1 Myr, the age of our pre-transitional disk sample, via the two leading theories of planet formation: the gas instability model and the core nucleated accretion model. In the gas instability model, fragmentation due to gravitational instabilities in the dense dust midplane (Goldreich & Ward 1973) can form Jupiter-mass clumps in the outer disk within a few hundred years (Boss 2000; Mayer et al. 2002; Durisen et al. 2007). According to the core nucleated accretion model (Pollack et al. 1996; Bodenheimer et al.

2000), dust grains will grow into planetesimals which will accrete other planetesimals and then form solid cores. These cores can become terrestrial planets or, if the cores are massive enough, gas giant cores which can accrete the surrounding gas in the disk (Pollack et al. 1996; Bodenheimer et al. 2000). For several years it was thought that the formation time for giant planets via core accretion was longer than the lifetime of disks, however, more recent simulations show that giant planets can form in the inner disk within ~ 1 Myr via two different mechanisms. One possible mechanism which could accelerate planet formation is migration. Alibert et al. (2005) found that a migrating core will not deplete its surrounding feeding zone and will reach its cross-over mass, the point at which the planet enters runaway gas accretion, sooner than found in previous models. Alternatively, the time to enter runaway gas accretion can be reduced by adopting low dust opacities (Pollack et al. 1996). A Jupiter-mass planet with a core of 10 Earth-masses can form at 5 AU in 1 Myr (Hubickyj et al. 2005), about half the time predicted by models using higher dust opacities.

It is likely that the pre-transitional disks originally had enough mass within their presently cleared regions to have formed multiple giant planets *in situ* and that planet formation may still be underway. Compared to a full disk with the same model parameters (Table 3), LkCa 15, UX Tau A, and Rox 44 are “missing” $10 M_{Jupiter}$, $40 M_{Jupiter}$, and $20 M_{Jupiter}$, respectively, some fraction of which could have gone into making giant planets. There is still enough material in the outer disk of these objects (Table 3) to potentially go into forming planets.

The next issue to address concerns the nature of the signatures that forming planets will leave behind in young disks. Theories predict that newly forming planets should clear the material around themselves through tidal disturbances leaving behind disk gaps (Goldreich & Tremaine 1980; Ward 1988; Rice et al. 2003; Paardekooper & Mellema 2004; Quillen et al. 2004; Varnière et al. 2006). To clear out the relatively large gaps we measure, it is likely that more than one planet is present and detailed simulations on the effects of multiple planets on the dust distribution are necessary. It is already known that when a stellar companion is located in the inner disk, the dust is dynamically cleared (Mathieu et al. 1991; Artymowicz & Lubow 1994). One example is the cavity in the inner disk of CoKu Tau/4 which is most likely due to clearing by its stellar companion (Ireland & Kraus 2008) and whose SED has been reproduced by a circumbinary disk model (Nagel et al. 2010). The object T54 in the Chamaeleon cloud is also a likely candidate for dust clearing by a stellar companion (Kim et al. 2009). These observations are evidence that dynamical dust clearing by companions does occur; the salient question is whether the companion in pre-transitional disks is in the stellar-mass or planet-mass regime. Searches for companions in the disks of UX Tau A and LkCa 15 have revealed that they are single stars down to 0.35 AU (Pott et al. 2010; White & Ghez 2001, A. Kraus, private communication). To explain the location of the outer walls of UX Tau A and LkCa 15, a stellar companion would have to be located at larger radii (Artymowicz & Lubow 1994), therefore we can conclude that the truncation of the outer disk is not due to

a stellar companion. Multiplicity studies of Rox 44 down to similar small radii do not yet exist.

If planets are clearing the dust in pre-transitional disks, we can speculate on the possible masses of such planets and their most likely formation scenario. Simulations of disk clearing demonstrate that Neptune-mass planets ($\sim 0.05 M_{Jupiter}$) can open gaps in the dust component of the disk while planets with $0.5 M_{Jupiter}$ can create a gap in the gas disk (Paardekooper & Mellema 2006). We can conjecture that the planets in the pre-transitional disks are between $0.05 M_{Jupiter}$ – $0.5 M_{Jupiter}$ based on the detection of a gap in their dust disks and evidence which suggests there are not substantial gaps in the gas disk. Since these disks are actively accreting, we can assume that gas travels from the outer disk to the inner disk and that therefore gas is located within the dust gap. In fact, in LkCa 15, UX Tau A, and Rox 44, gas has been detected within the dust gap (Najita et al. 2003; Salyk et al. 2009). These partially-filled gas gaps have consequences on Type II migration. According to classical Type II migration, planets will migrate inward onto the star on the viscous timescale, followed by the outer disk edge, and therefore we would not see gaps on these short timescales (Lin & Papaloizou 1986). The gap in the gas disk in the above scenario is deep and there is no gas flow across it. However, Crida & Morbidelli (2007) showed that inward planet migration can be slowed or stopped if the gap is not completely cleared of gas. In this case, the gas in the gap will exert a positive torque on the outer disk which diminishes the total torque that the planet feels from the outer disk. As a result the outer disk will not migrate the planet inward as quickly, opening the possibility that planets can sustain gaps in disks long enough for us to detect them. Based on the points above, it follows that the planets in pre-transitional disks were most likely formed via core accretion since gravitational instability tends to form planets of several Jupiter masses in the outermost disk, and moreover, these planets would have needed to migrate to the inner disk to form the gaps we are detecting.

The alternative disk clearing mechanisms proposed to date have difficulties explaining several observations and are most likely not responsible for the type of clearing seen in pre-transitional disks. Grain growth simulations predict that dust will evolve on faster timescales in the inner parts of the disk, and eventually the small grains which contribute to the near-IR emission of the disk will grow causing a flux deficit in the SED (Dullemond & Dominik 2004, 2005). However, the gap edges and silicate features are too sharp to be explained by grain growth. In addition, grain growth is an inside-out clearing mechanism and does not account for a remnant inner disk.

In the MRI clearing scenario, X-rays from the star can activate the MRI in the ionized inner wall of the disk which will lead material to accrete from the wall onto the star, creating a hole in the disk that grows outward (Chiang & Murray-Clay 2007). It predicts a stronger trend of gap size with X-ray luminosity and accretion rate than is observed (Kim et al. 2009) and requires an inner disk hole, not a gap, to already exist before it can take effect.

Radiation from the central star can potentially photo-evaporate the surrounding disk (Hollenbach et al. 1994;

Clarke et al. 2001). High energy photons from the stellar wind will impinge upon the upper disk layers. As the disk evolves viscously, the mass accretion rate decreases with time, eventually reaching the mass loss rate in the photoevaporative wind. At this point, the photoevaporative wind takes over and inward accretion onto the star will essentially stop. Once the isolated inner disk drains onto the star on the viscous timescale, the inner edge of the outer disk will be directly irradiated by the star and the hole will keep growing outward (Alexander & Armitage 2007). The typical value of the mass loss rate in the photoevaporative wind was typically taken to be $\sim 4 \times 10^{-10} M_{\odot} \text{ yr}^{-1}$ based on EUV radiation alone (Clarke et al. 2001), however, this value has recently jumped to $\sim 10^{-8} M_{\odot} \text{ yr}^{-1}$ due to the inclusion of X-ray and UV photons (Gorti & Hollenbach 2009; Owen et al. 2010). However, if mass loss rates are as high as this value it poses significant problems. The average mass accretion rate measured in TTS is $\sim 10^{-8} M_{\odot} \text{ yr}^{-1}$ (Hartmann et al. 1998). According to the evolutionary scenario outlined above, it follows that we should not see disks with mass accretion rates lower than this value, in contrast to what is observed (Hartmann et al. 1998). Moreover, modeling of disk wind indicators (i.e. forbidden line profiles) by Hartigan et al. (1995) find that the winds of TTS are typically ~ 0.01 of the mass accretion rate. In any case, photoevaporation opens short-lived gaps in the disk that would not lead to a discernible deficit in the SED (see § 5.1), and the models presented to date are not compatible with large 40 – 50 AU gaps in massive disks which are still actively accreting. Furthermore, due to shadowing, there are portions of the outer wall that will not be affected by the photoevaporative wind.

Given the detection of over one hundred Jupiter-mass planets (Butler et al. 2006) and about one dozen Neptune-mass planets (see references within Endl et al. (2008)), it is natural to wonder if we can see evidence for the incipient stages of planet formation and particularly if pre-transitional disks around TTS constitute such evidence. At the moment, *ALMA* is the best suited facility to detect disks around young planets within TTS disks (Wolf & D’Angelo 2005) and therefore search for planets within the gaps of pre-transitional disks. *ALMA*, along with *JWST*, will help us to better constrain the statistics of pre-transitional disks and their evolution. High-resolution near-IR interferometry can also examine the inner disk and reveal the spatial distribution of the optically thin dust within the disk gap.

6. SUMMARY & CONCLUSIONS

In this paper we presented spectral type measurements as well as veiling and near-infrared excess measurements for the diskless LkCa 14, the pre-transitional disks of LkCa 15, UX Tau A, and Rox 44, and the transitional disks of DM Tau and GM Aur. Using near-IR SpeX

spectra from 1–5 μm , we extracted the near-IR excess continua of our pre-transitional disk sample and fit their excess emission with optically thick inner disk walls, supporting the interpretation that these objects contain gaps in their disks. We modeled the broad-band SEDs of these pre-transitional disks and measure gap sizes of $\sim 40\text{--}70$ AU. In the case of LkCa 15 and Rox 44 there is $\sim 10^{-11} M_{\odot}$ of ISM-sized optically thin dust within the gap.

The near-infrared emission of our pre-transitional disks differs significantly from that of the transitional disks of DM Tau and GM Aur. DM Tau has no veiling and no excess emission in the near-IR, indicating that its disk hole is relatively empty of small dust grains. GM Aur has a small amount of veiling and displays a flat excess above the stellar photosphere in the near-IR, which can be fit by a model of optically thin dust emission. This is in contrast to the pre-transitional disks which have large, blackbody-like near-IR excess continua that can be fit with models of a wall located at the dust sublimation radius.

We also studied the effects of shadowing of the outer disk wall by the inner disk. We found that when the finite size of the star is taken into account, a significant portion of the outer wall is either in the penumbra or completely out of the shadow of the inner wall. The predicted height of the wall is consistent with that of the outer disk, which is derived independently.

Based on currently known disk clearing mechanisms, we propose that the gaps in pre-transitional disks are indicators of planet formation, making these disks a promising location for young planet searches. *ALMA* will be pivotal in extending the sample of known pre-transitional disks and has the potential to detect planets in these gaps. Near-IR interferometry will play an important role in further understanding the innermost regions of these disks. Future studies of this class of objects may bring us a few steps closer to understanding the origin of our own solar system.

We thank Cesar Briceño and Scott Kenyon for kindly providing the FAST spectra used in this paper. We also thank Perry Berlind for performing the FAST observations. We thank Sean Andrews and David Wilner for useful discussions. The near-infrared spectra used in this paper were obtained using SpeX at the Infrared Telescope Facility, which is operated by the University of Hawaii under Cooperative Agreement no. NNX08AE38A with the National Aeronautics and Space Administration, Science Mission Directorate, Planetary Astronomy Program. C. E. was supported by the National Science Foundation under Award No. 0901947. P. D. acknowledges a grant from PAPIIT-DGAPA UNAM. E. N. thanks a postdoctoral fellowship from Conacyt. K. L. was supported by grant AST-0544588 from the National Science Foundation. N. C. acknowledges support from NASA Origins Grant NNX08AH94G.

APPENDIX

THE EFFECT OF DISK SHADOWING

A point source does not cast a penumbra. It only casts an umbra with a size, measured from above the midplane, of

$$z_{point} = z_w \frac{r}{r_w} \quad (\text{A1})$$

where z_w is the height of the inner wall above the midplane, r_w is the radial distance between the center of the star and the inner wall, and r is the radius of the outer wall as measured from the center of the star.

However, since the star is a finite source, the size of the umbra will be much smaller. At the outer wall, the height over which the whole star can be seen and the height below which the star cannot be seen are calculated using the roots of a quadratic function. This function is constructed for the distance between the inner wall and the points where rays tangent to the upper and lower parts of the star and the upper part of the inner wall cross the horizontal plane (Figure 14). Using dimensionless distances (with R_* as unity)

$$x^+ = (r_w + \sqrt{(1 + \frac{1}{z_w})(1 - \frac{1}{z_w}) + \frac{r_w^2}{z_w^2}}) / [(1 + \frac{1}{z_w})(1 - \frac{1}{z_w})], \quad (\text{A2})$$

$$x^- = (r_w - \sqrt{(1 + \frac{1}{z_w})(1 - \frac{1}{z_w}) + \frac{r_w^2}{z_w^2}}) / [(1 + \frac{1}{z_w})(1 - \frac{1}{z_w})], \quad (\text{A3})$$

$$z_v^+ = (r - r_w)(z_w/x^-) + z_w, \quad (\text{A4})$$

$$z_v^- = (r - r_w)(z_w/x^-) + z_w, \quad (\text{A5})$$

and, consequently, the outer wall above z_v^- will be illuminated to some degree.

Given that a significant portion of the outer wall is not fully illuminated by the star, we consider the effect of the shadow, both the umbra and penumbra, on the heating of the wall and hence the resulting emission. The solid angle subtended by the star as seen by any point P in the disk, with coordinates r and z , is

$$\Omega_*(r, z) = 2 \int_0^{\theta_{max}} \int_0^{\phi_{max}} \sin\phi d\phi d\theta \quad (\text{A6})$$

where ϕ characterizes an annulus at the stellar surface, and θ allows one to integrate over the annulus. The maximum value of ϕ is

$$\phi_{max} = \sin^{-1}(1/d) \quad (\text{A7})$$

where

$$d = (z^2 + r^2)^{1/2}. \quad (\text{A8})$$

The maximum value of θ depends on the shadow.

In Figure 15 we show the relevant angles used to define the integration limits of the solid angle of the star. The angle γ is related to the height of the shadow. If $\phi < \gamma$ the whole annulus can be seen, and then $\theta_{max} = \pi$. However, if $\phi > \gamma$ then a fraction of the annulus is in the shadow.

From the figure, we can see that

$$\theta_{max} = \pi - E \quad (\text{A9})$$

and

$$h = \sin \beta \cos E. \quad (\text{A10})$$

To find the angle β we use that

$$\sin \beta = c \sin \phi \quad (\text{A11})$$

and

$$c = d \cos \phi - \sqrt{1 - (d \sin \phi)^2}. \quad (\text{A12})$$

Then, β is given by

$$\sin \beta = d \cos \phi \sin \phi - [1 - (d \sin \phi)^2]^{1/2} \sin \phi. \quad (\text{A13})$$

The other relevant angle γ , is given by $\gamma = A - B$, and so

$$\gamma = \tan^{-1}(r/z) - \tan^{-1}[(r - r_w)/(z - z_w)]. \quad (\text{A14})$$

The height h is given by

$$h = (d - \cos \beta) \tan \gamma \quad (\text{A15})$$

and thus,

$$\cos E = (d - \cos \beta) \tan \gamma / \sin \beta, \quad (\text{A16})$$

which is used in Eq. A9 to calculate θ_{max} , which in turn allows one to calculate the solid angle, Ω_* , with Eq. A6.

REFERENCES

- Alexander, R. D., & Armitage, P. J. 2007, MNRAS, 375, 500
 Alibert, Y., Mordasini, C., Benz, W., & Winisdoerffer, C. 2005, A&A, 434, 343

- Andrews, S. M., & Williams, J. P. 2005, *ApJ*, 631, 1134
- Andrews, S. M., Wilner, D. J., Hughes, A. M., Qi, C., & Dullemond, C. P. 2009, *ApJ*, 700, 1502
- Artymowicz, P., & Lubow, S. H. 1994, *ApJ*, 421, 651
- Begemann, B., Dorschner, J., Henning, T., Mutschke, H., & Thamm, E. 1994, *ApJ*, 423, L71
- Bergin, E., et al. 2004, *ApJ*, 614, L133
- Bodenheimer, P., Hubickyj, O., & Lissauer, J. J. 2000, *Icarus*, 143, 2
- Boss, A. P. 2000, *ApJ*, 536, L101
- Bouvier, J., & Appenzeller, I. 1992, *A&AS*, 92, 481
- Butler, R. P., et al. 2006, *ApJ*, 646, 505
- Calvet, N., D'Alessio, P., Hartmann, L., Wilner, D., Walsh, A., & Sitko, M. 2002, *ApJ*, 568, 1008
- Calvet, N., & Gullbring, E. 1998, *ApJ*, 509, 802
- Calvet, N., Magris, G. C., Patino, A., & D'Alessio, P. 1992, *Revista Mexicana de Astronomia y Astrofisica*, 24, 27
- Calvet, N., Patino, A., Magris, G. C., & D'Alessio, P. 1991, *ApJ*, 380, 617
- Calvet, N., et al. 2005, *ApJ*, 630, L185
- Chiang, E., & Murray-Clay, R. 2007, *Nature Physics*, 3, 604
- Clarke, C. J., Gendrin, A., & Sotomayor, M. 2001, *MNRAS*, 328, 485
- Cohen, M., & Kuhl, L. V. 1979, *ApJS*, 41, 743
- Crida, A., & Morbidelli, A. 2007, *MNRAS*, 377, 1324
- Cushing, M. C., Rayner, J. T., & Vacca, W. D. 2005, *ApJ*, 623, 1115
- Cushing, M. C., Vacca, W. D., & Rayner, J. T. 2004, *PASP*, 116, 362
- D'Alessio, P., Calvet, N., Hartmann, L., Franco-Hernández, R., & Servín, H. 2006, *ApJ*, 638, 314
- D'Alessio, P., Calvet, N., Hartmann, L., Lizano, S., & Cantó, J. 1999, *ApJ*, 527, 893
- D'Alessio, P., et al. 2005, *ApJ*, 621, 461
- Dorschner, J., Begemann, B., Henning, T., Jaeger, C., & Mutschke, H. 1995, *A&A*, 300, 503
- Draine, B. T., & Lee, H. M. 1984, *ApJ*, 285, 89
- Dullemond, C. P., & Dominik, C. 2004, *A&A*, 421, 1075
- . 2005, *A&A*, 434, 971
- Durisen, R. H., Boss, A. P., Mayer, L., Nelson, A. F., Quinn, T., & Rice, W. K. M. 2007, in *Protostars and Planets V*, ed. B. Reipurth, D. Jewitt, & K. Keil, 607–622
- Edwards, S., Fischer, W., Hillenbrand, L., & Kwan, J. 2006, *ApJ*, 646, 319
- Endl, M., Cochran, W. D., Wittenmyer, R. A., & Boss, A. P. 2008, *ApJ*, 673, 1165
- Espaillet, C. 2009, PhD thesis, University of Michigan
- Espaillet, C., Calvet, N., D'Alessio, P., Hernández, J., Qi, C., Hartmann, L., Furlan, E., & Watson, D. M. 2007a, *ApJ*, 670, L135
- Espaillet, C., Calvet, N., Luhman, K. L., Muzerolle, J., & D'Alessio, P. 2008a, *ApJ*, 682, L125
- Espaillet, C., et al. 2007b, *ApJ*, 664, L111
- . 2008b, *ApJ*, 689, L145
- Evans, N. J., et al. 2009, *ApJS*, 181, 321
- Fabricant, D., Cheimets, P., Caldwell, N., & Geary, J. 1998, *PASP*, 110, 79
- Folha, D. F. M., & Emerson, J. P. 1999, *A&A*, 352, 517
- Furlan, E., et al. 2006, *ApJS*, 165, 568
- . 2009, *ApJ*, 703, 1964
- Goldreich, P., & Tremaine, S. 1980, *ApJ*, 241, 425
- Goldreich, P., & Ward, W. R. 1973, *ApJ*, 183, 1051
- Gorti, U., & Hollenbach, D. 2009, *ApJ*, 690, 1539
- Gullbring, E., Hartmann, L., Briceño, C., & Calvet, N. 1998, *ApJ*, 492, 323
- Hartigan, P., Edwards, S., & Ghandour, L. 1995, *ApJ*, 452, 736
- Hartigan, P., Hartmann, L., Kenyon, S., Hewett, R., & Stauffer, J. 1989, *ApJS*, 70, 899
- Hartigan, P., Strom, K. M., & Strom, S. E. 1994, *ApJ*, 427, 961
- Hartmann, L., Calvet, N., Gullbring, E., & D'Alessio, P. 1998, *ApJ*, 495, 385
- Herbig, G. H. 1977, *ApJ*, 214, 747
- Herbig, G. H., Vrba, F. J., & Rydgren, A. E. 1986, *AJ*, 91, 575
- Herbst, W., Herbst, D. K., Grossman, E. J., & Weinstein, D. 1994, *AJ*, 108, 1906
- Hernández, J., Calvet, N., Briceño, C., Hartmann, L., & Berlind, P. 2004, *AJ*, 127, 1682
- Høg, E., et al. 2000, *A&A*, 355, L27
- Hollenbach, D., Johnstone, D., Lizano, S., & Shu, F. 1994, *ApJ*, 428, 654
- Houck, J. R., et al. 2004, *ApJS*, 154, 18
- Hubickyj, O., Bodenheimer, P., & Lissauer, J. J. 2005, *Icarus*, 179, 415
- Hughes, A. M., et al. 2009, *ApJ*, 698, 131
- Ireland, M. J., & Kraus, A. L. 2008, *ApJ*, 678, L59
- Karr, J. L., Ohashi, N., Kudo, T., & Tamura, M. 2010, *AJ*, 139, 1015
- Kenyon, S. J., Brown, D. I., Tout, C. A., & Berlind, P. 1998, *AJ*, 115, 2491
- Kenyon, S. J., & Hartmann, L. 1995, *ApJS*, 101, 117
- Kim, K. H., et al. 2009, *ApJ*, 700, 1017
- Lin, D. N. C., & Papaloizou, J. 1986, *ApJ*, 309, 846
- Lubow, S. H., & D'Angelo, G. 2006, *ApJ*, 641, 526
- Luhman, K. L., Allen, P. R., Espaillet, C., Hartmann, L., & Calvet, N. 2010, *ApJS*, 186, 111
- Mathieu, R. D., Adams, F. C., & Latham, D. W. 1991, *AJ*, 101, 2184
- Mathis, J. S. 1990, *ARA&A*, 28, 37
- Mathis, J. S., Rumpl, W., & Nordsieck, K. H. 1977, *ApJ*, 217, 425
- Mayer, L., Quinn, T., Wadsley, J., & Stadel, J. 2002, *Science*, 298, 1756
- McClure, M. K., et al. 2010, submitted
- Monnier, J. D., & Millan-Gabet, R. 2002, *ApJ*, 579, 694
- Mulders, G. D., Dominik, C., & Min, M. 2010, *ArXiv e-prints (arXiv:1001.2146)*
- Muzerolle, J., Calvet, N., Hartmann, L., & D'Alessio, P. 2003, *ApJ*, 597, L149
- Muzerolle, J., D'Alessio, P., Calvet, N., & Hartmann, L. 2004, *ApJ*, 617, 406
- Muzerolle, J., et al. 2009, *ApJ*, 704, L15
- Nagel, E., D'Alessio, P., Calvet, N., Espaillet, C., Sargent, B., Hernández, J., & Forrest, W. J. 2010, *ApJ*, 708, 38

- Najita, J., Carr, J. S., & Mathieu, R. D. 2003, *ApJ*, 589, 931
- Norton, A. J., et al. 2007, *A&A*, 467, 785
- Nuernberger, D., Brandner, W., Yorke, H. W., & Zinnecker, H. 1998, *A&A*, 330, 549
- Owen, J. E., Ercolano, B., Clarke, C. J., & Alexander, R. D. 2010, *MNRAS*, 401, 1415
- Paardekooper, S., & Mellema, G. 2006, *A&A*, 459, L17
- Paardekooper, S.-J., & Mellema, G. 2004, *A&A*, 425, L9
- Padgett, D. L., et al. 2008, *ApJ*, 672, 1013
- Piétu, V., Dutrey, A., Guilloteau, S., Chapillon, E., & Pety, J. 2006, *A&A*, 460, L43
- Pollack, J. B., Hollenbach, D., Beckwith, S., Simonelli, D. P., Roush, T., & Fong, W. 1994, *ApJ*, 421, 615
- Pollack, J. B., Hubickyj, O., Bodenheimer, P., Lissauer, J. J., Podolak, M., & Greenzweig, Y. 1996, *Icarus*, 124, 62
- Pott, J., Perrin, M. D., Furlan, E., Ghez, A. M., Herbst, T. M., & Metchev, S. 2010, *ApJ*, 710, 265
- Quillen, A. C., Blackman, E. G., Frank, A., & Varnière, P. 2004, *ApJ*, 612, L137
- Rayner, J. T., Cushing, M. C., & Vacca, W. D. 2009, *ApJS*, 185, 289
- Rayner, J. T., Toomey, D. W., Onaka, P. M., Denault, A. J., Stahlberger, W. E., Vacca, W. D., Cushing, M. C., & Wang, S. 2003, *PASP*, 115, 362
- Rice, W. K. M., Armitage, P. J., Wood, K., & Lodato, G. 2006, *MNRAS*, 373, 1619
- Rice, W. K. M., Wood, K., Armitage, P. J., Whitney, B. A., & Bjorkman, J. E. 2003, *MNRAS*, 342, 79
- Rydgren, A. E., Strom, S. E., & Strom, K. M. 1976, *ApJS*, 30, 307
- Salyk, C., Blake, G. A., Boogert, A. C. A., & Brown, J. M. 2007, *ApJ*, 655, L105
- . 2009, *ApJ*, 699, 330
- Siess, L., Dufour, E., & Forestini, M. 2000, *A&A*, 358, 593
- Simon, M., Dutrey, A., & Guilloteau, S. 2000, *ApJ*, 545, 1034
- Skrutskie, M. F., et al. 2006, *AJ*, 131, 1163
- Strom, K. M., Strom, S. E., Edwards, S., Cabrit, S., & Skrutskie, M. F. 1989, *AJ*, 97, 1451
- Vacca, W. D., Cushing, M. C., & Rayner, J. T. 2003, *PASP*, 115, 389
- Varnière, P., Blackman, E. G., Frank, A., & Quillen, A. C. 2006, *ApJ*, 640, 1110
- Ward, W. R. 1988, *Icarus*, 73, 330
- Warren, S. G. 1984, *Appl. Opt.*, 23, 1206
- Weaver, W. B., & Jones, G. 1992, *ApJS*, 78, 239
- Werner, M. W., et al. 2004, *ApJS*, 154, 1
- White, R. J., & Ghez, A. M. 2001, *ApJ*, 556, 265
- Wolf, S., & D'Angelo, G. 2005, *ApJ*, 619, 1114

Table 1
Log of SpeX Observations

Target	K_s^1	Date	LXD Exposure (s)	SNR ²
LkCa 14	8.6	2009 Feb 18	1800	270
LkCa 15	8.2	2009 Dec 22	2400	370
UX Tau A	7.6	2009 Dec 22	2400	450
Rox 44	7.6	2009 Apr 07	1800	150
GM Aur	8.3	2009 Dec 22	2400	300
DM Tau	9.5	2009 Feb 16	2400	170

¹ Two-Micron All-Sky Survey Point Source Catalog (2MASS; Skrutskie et al. 2006)

² Measured at $\sim 2.2 \mu\text{m}$.

Table 2
Characteristics of Sample

Target	Spectral Type	r_K	T_{wall}^i (K) ¹	Disk Class ²
LkCa 14	K5.5	0	...	diskless
LkCa 15	K3	0.6	1400	pTD
UX Tau A	G8	0.4	1550	pTD
Rox 44	K3 ³	0.8	1200	pTD
GM Aur	K5.5	0.1	...	TD
DM Tau	M1.5	0	...	TD

¹ T_{wall}^i refers to the temperature of the best-fit wall to the the excess near-IR emission, if present.

² Our targets are classified as diskless stars, stars with transitional disks (TD), and stars with pre-transitional disks (pTD).

³ Value adopted from Bouvier & Appenzeller (1992).

Table 3
Stellar and Model Properties
of LkCa 15, UX Tau A, & Rox 44

Stellar Properties			
	LkCa 15	UX Tau A	Rox 44
M_* (M_\odot)	1.3	1.5	1.3
R_* (R_\odot)	1.6	1.8	1.6
T_* (K)	4730	5520	4730
\dot{M} ($M_\odot \text{ yr}^{-1}$)	3.3×10^{-9}	1.1×10^{-8}	9.3×10^{-9}
Inclination (deg)	42 ¹	60	45 ²
Distance (pc)	140	140	120
A_V	1.7	1.8	2.2
Optically Thick Inner Wall			
a_{max} (μm)	1	10	1
T_{wall}^i (K)	1400	1550	1200
z_{wall}^i (AU)	0.017	0.009	0.034
R_{wall}^i (AU)	0.15	0.15	0.25
Optically Thick Inner Disk			
$R_{inner \text{ disk}}$ (AU)	< 0.19	< 0.21	< 0.4
$M_{inner \text{ disk}}$ (M_\odot)	$< 2 \times 10^{-4}$	$< 6 \times 10^{-5}$	$< 8 \times 10^{-5}$
Optically Thick Outer Wall			
a_{max} (μm)	0.25	0.25	0.25
T_{wall}^o (K) ³	95	110	120
z_{wall}^o (AU)	12.9	13.8	9.9
R_{wall}^o (AU) ³	58	71	36
Optically Thick Outer Disk			
ϵ	0.001	0.001	0.01
α	0.0005	0.004	0.006
M_{disk} (M_\odot)	0.1	0.04	0.03

¹ Simon et al. (2000)

² Andrews et al. (2009)

³ Since we take into account the varying illumination along the outer wall due to the shadowing, there will be a range of T_{wall}^o . Here we report the temperature of the fully illuminated part of the wall and use this value to calculate R_{wall}^o .

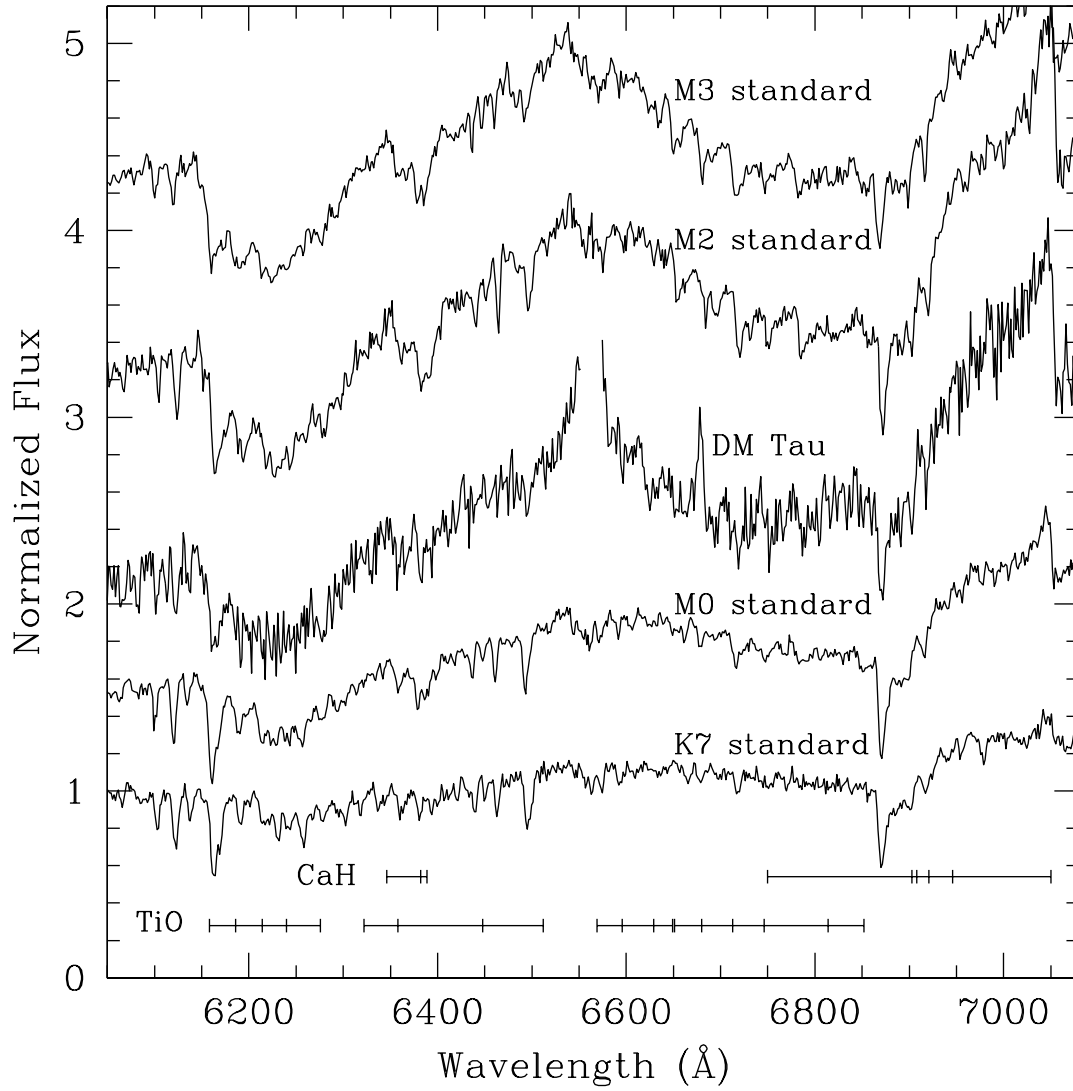


Figure 1. FAST spectrum of DM Tau compared to spectral type standards. We measure a spectral type of $M1.5 \pm 1$ for DM Tau. Some of the features used for spectral classification are marked. The strong H_{α} emission feature at ~ 6550 Å is cut off for clarity.

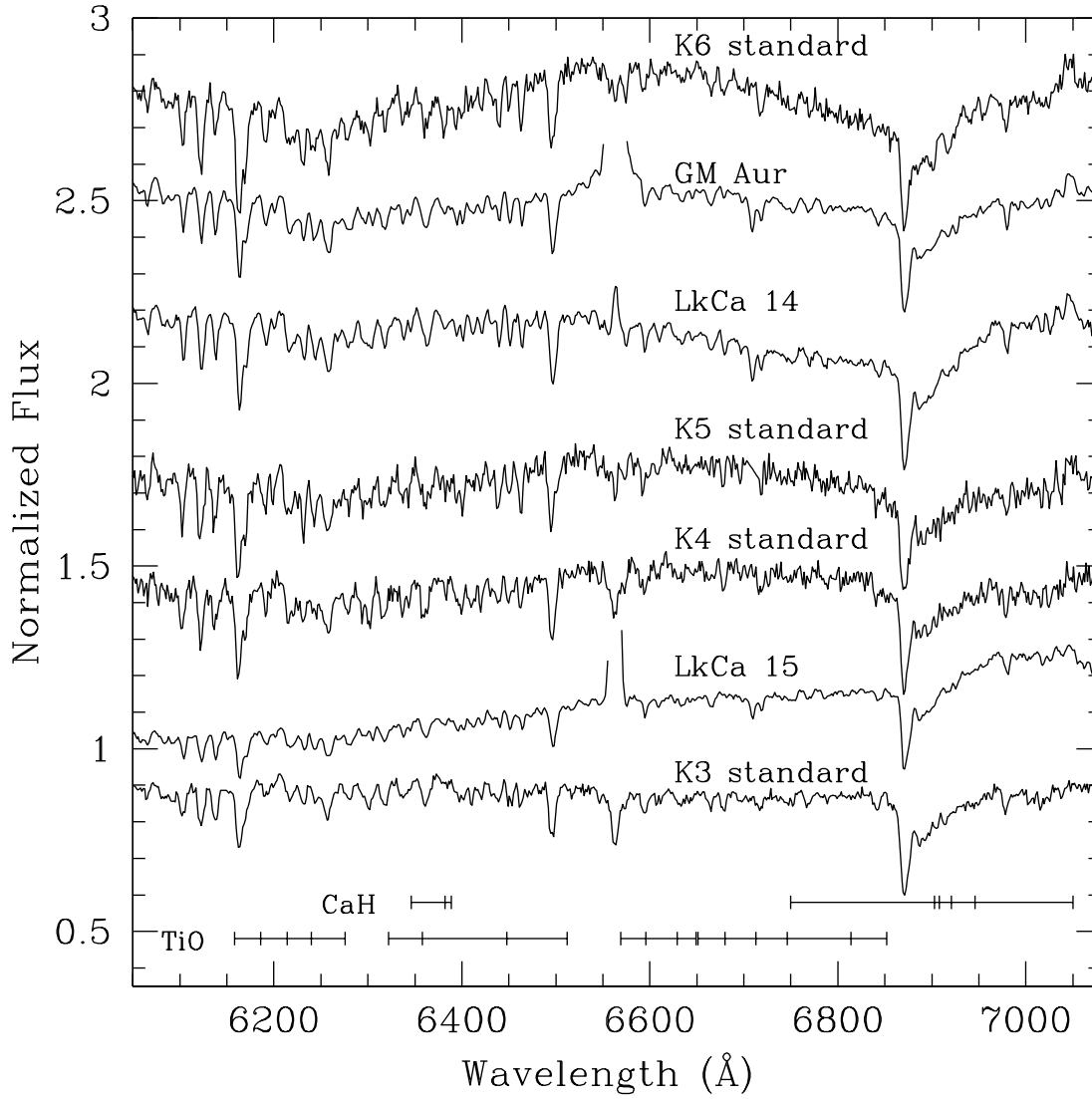


Figure 2. FAST spectra of GM Aur, LkCa 14, and LkCa 15 compared to spectral type standards. We measure a spectral type of $K5.5 \pm 1$ for both GM Aur and LkCa 14 and a spectral type of $K3 \pm 1$ for LkCa 15. Some of the features used for spectral classification are marked. The strong $H\alpha$ emission features at ~ 6550 Å in GM Aur and LkCa 15 have been trimmed.

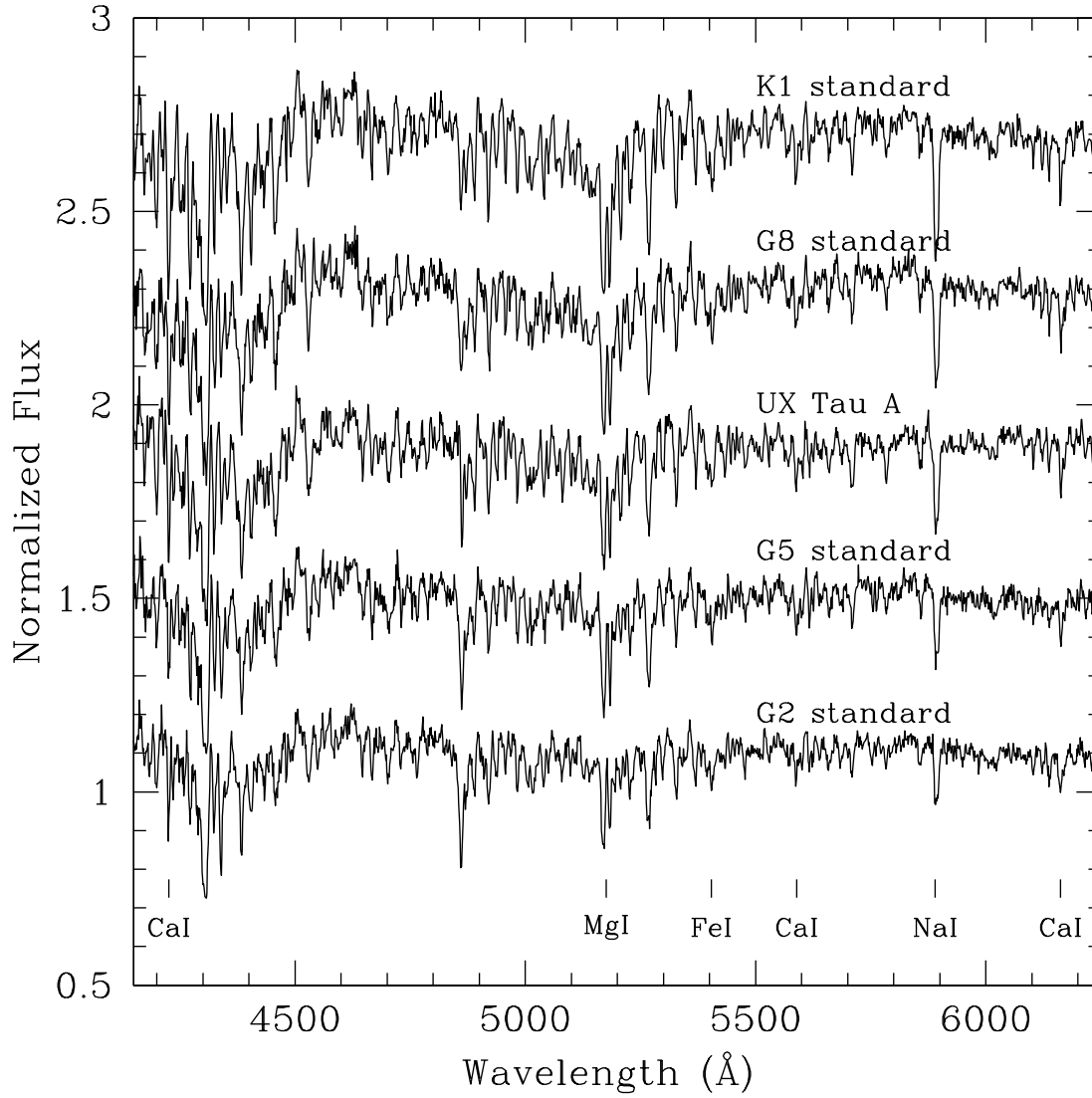


Figure 3. FAST spectrum of UX Tau A compared to spectral type standards. We measure a spectral type of $G8\pm 2$ for UX Tau A. Some of the features used for spectral classification are marked.

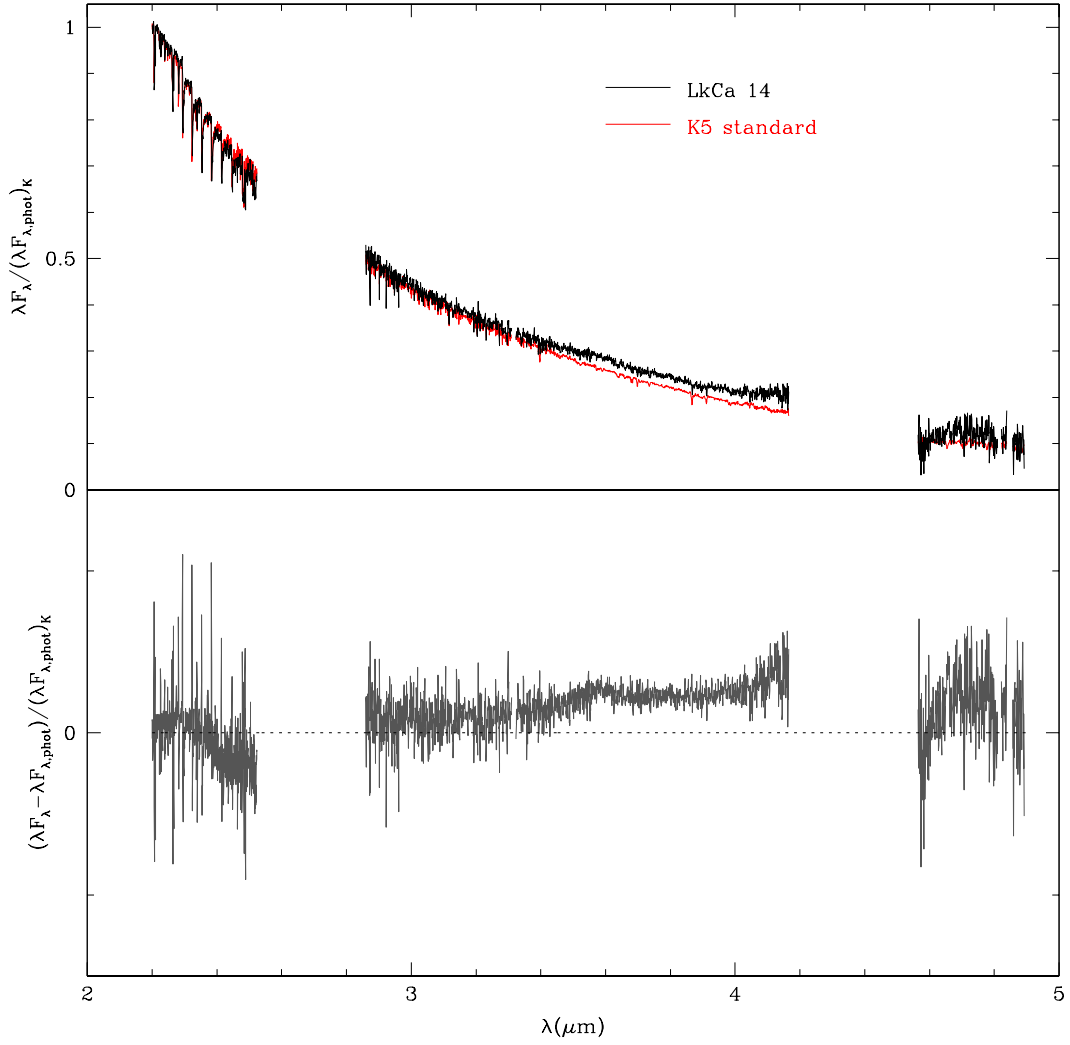


Figure 4. Near-infrared emission of the diskless T Tauri star LkCa 14 relative to a standard star. The top panel contains the SpeX spectrum of LkCa 14 (dark line) compared to a K5 standard (light line). LkCa 14 has absorption lines that are not veiled relative to the standard star and we derive a veiling value (τ_K) of 0 for LkCa 14 between $2.20 - 2.28 \mu\text{m}$. The bottom panel displays the near-infrared excess emission of LkCa 14. After we subtract the standard star from the target (bottom), we find that there is no excess emission above the photosphere of LkCa 14 (gray). The dotted line corresponds to no excess and the small discrepancy between $\sim 3.5 - 4.2 \mu\text{m}$ is likely due to spectral slope uncertainties. This indicates that SpeX spectra of dwarfs are good templates for the photospheres of young stars.

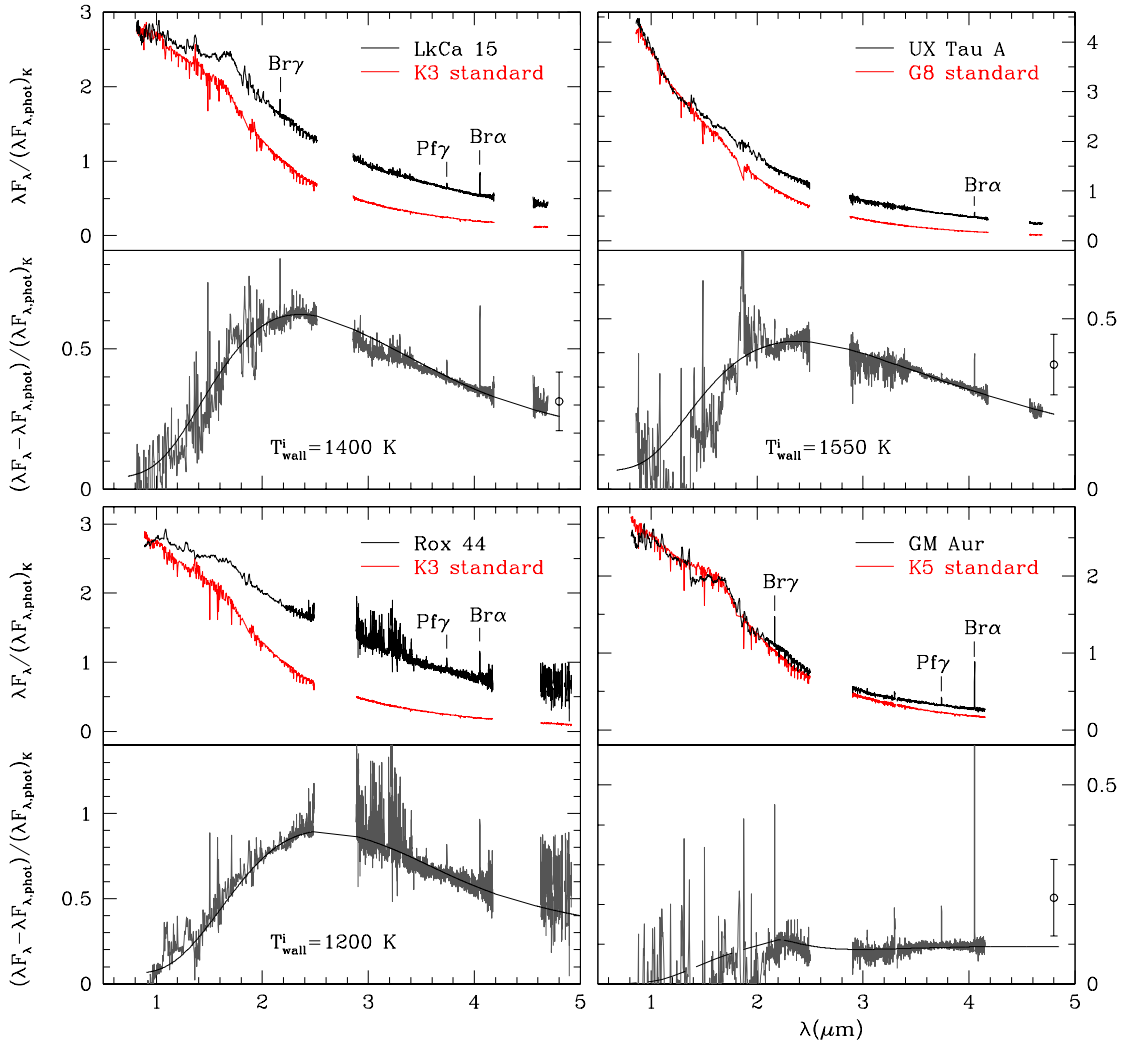


Figure 5. SpeX near-infrared emission of the pre-transitional disks of LkCa 15, UX Tau A, and Rox 44 and the transitional disk of GM Aur relative to a standard star. After scaling the targets by $1 + r_K$, we subtracted the standard star spectra (top, light line) from the veiling-scaled target spectra (top, dark line) to extract the shapes of the excess emission above the photosphere (bottom, gray). We measure an r_K of 0.6, 0.4, 0.8, and 0.1 for LkCa 15, UX Tau A, Rox 44, and GM Aur, respectively. Additional veiling measurements from Salyk et al. (2009) at $\sim 4.8 \mu\text{m}$ (open points) are shown. For the pre-transitional disks, we find that the near-infrared excess emission can be reproduced by the wall of an optically thick inner disk with a temperature of T_{wall}^i (solid line). In the case of GM Aur, we can reproduce the near-IR excess emission with an optically thin dust model (bottom, broken line) composed of sub-micron-sized dust located within the inner disk hole following Calvet et al. (2005). We note that GM Aur was too faint to extract any data at wavelengths greater than $\sim 4.2 \mu\text{m}$ and that, in each of the spectra, regions from $\sim 1.2\text{--}1.4 \mu\text{m}$, $\sim 1.8\text{--}1.9 \mu\text{m}$, and $\sim 2.8\text{--}3.2 \mu\text{m}$ are strongly affected by uncertainties in the telluric subtraction.

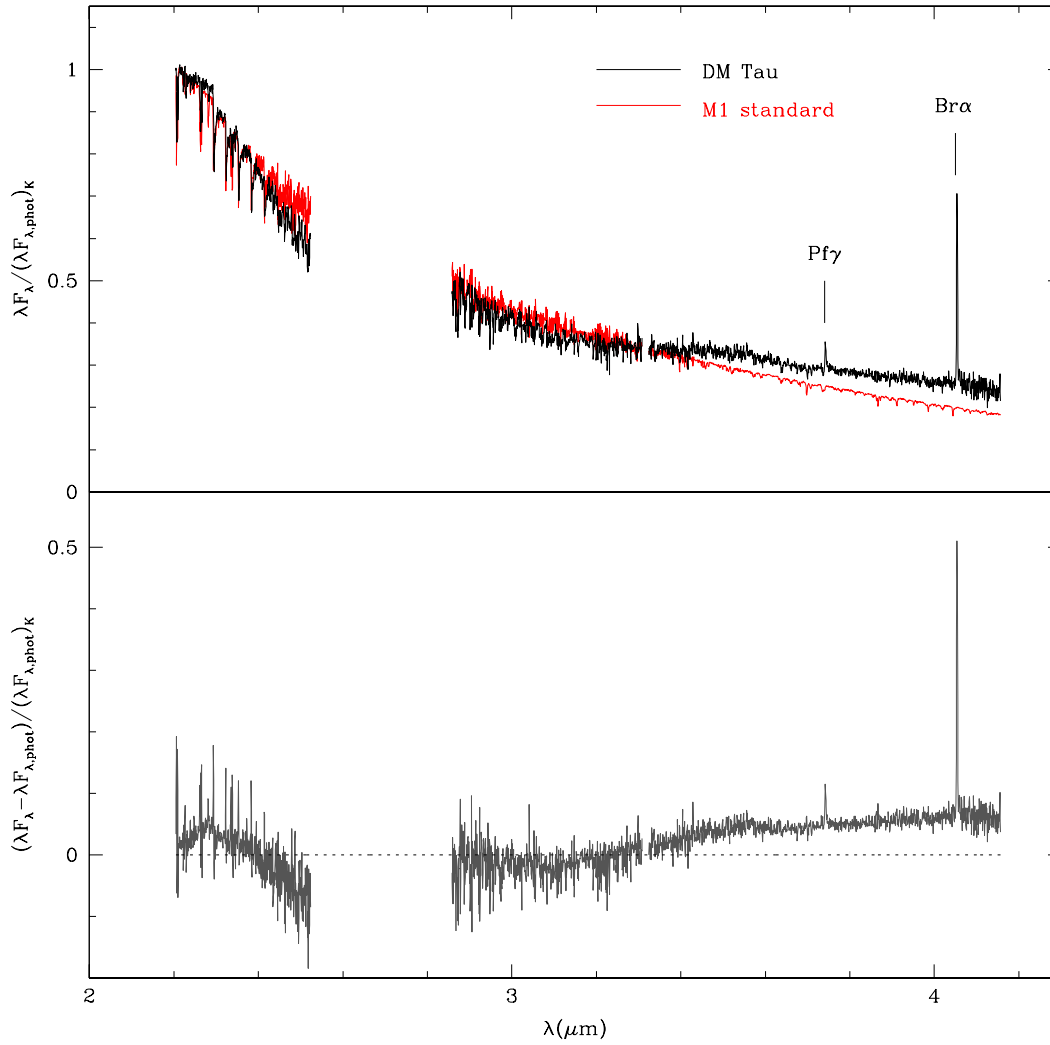


Figure 6. Near-infrared emission of the transitional disk of DM Tau relative to a standard star. In the top panel, we compare the SpeX spectrum of DM Tau (solid line) to a M1 dwarf standard star (broken line). We derive $r_K=0$ for DM Tau between $2.20 - 2.28 \mu\text{m}$ and find that after subtracting the standard from the target (bottom panel) there is also no excess at longer wavelengths. The dotted line in the bottom panel corresponds to zero excess. The small discrepancy between $\sim 2.4-2.5 \mu\text{m}$ is likely due to spectral slope uncertainties. Note that DM Tau was too faint to extract any data at wavelengths greater than $\sim 4.2 \mu\text{m}$.

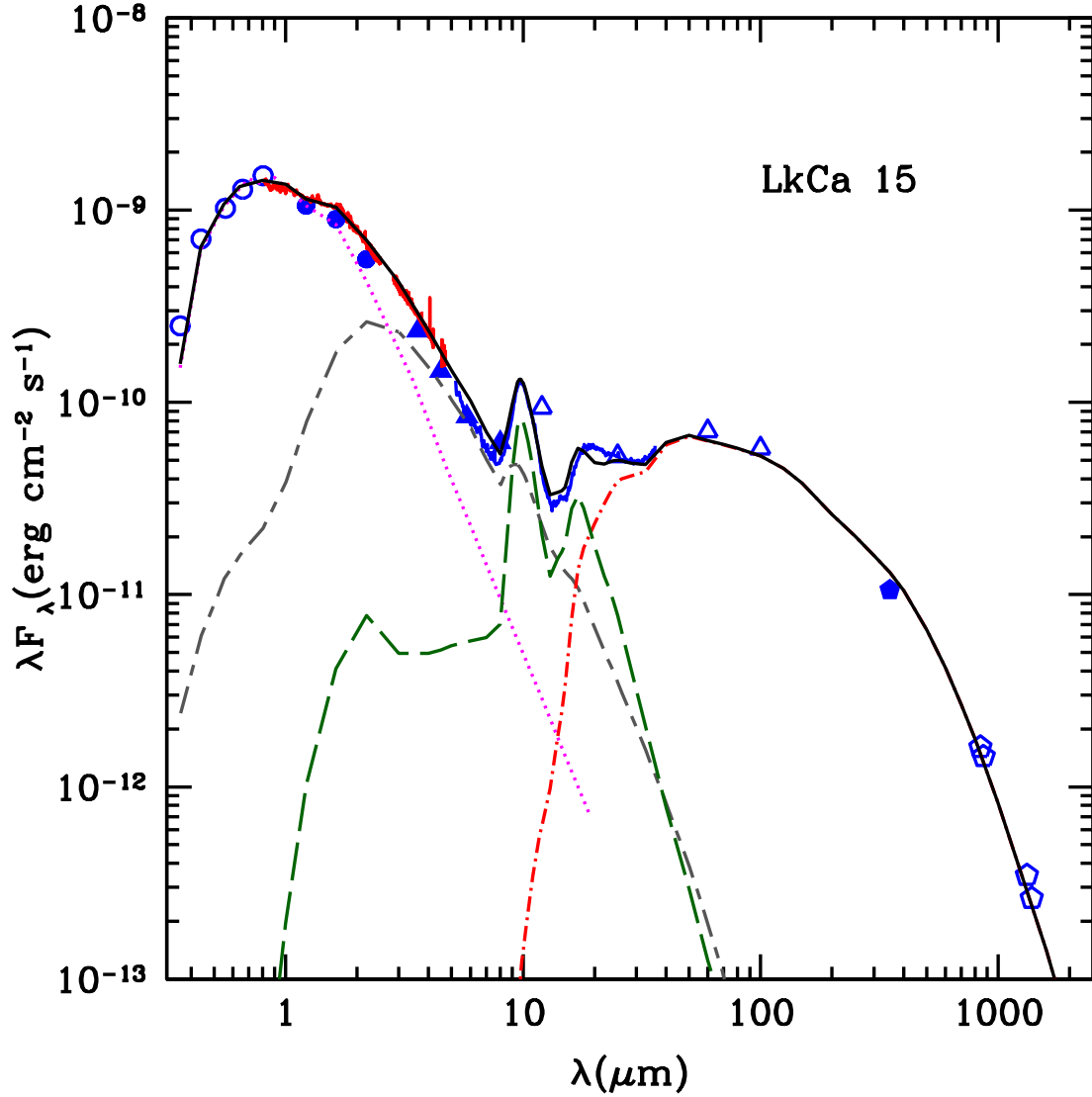


Figure 7. Pre-transitional disk model of LkCa 15. The best-fit model to LkCa 15 (solid black line) consists of an inner optically thick disk which extends from the dust destruction radius to <0.26 AU and an outer disk from 58 – 300 AU. Within the inner 4 AU of the gap between the inner and outer disk, there is $\sim 10^{-11} M_{\odot}$ of ISM-sized optically thin dust. Separate model components are the stellar photosphere (magenta dotted line; Kenyon & Hartmann 1995), the inner disk (gray short-long-dash), the outer disk (red dot-short-dash), and the optically thin small dust located within the disk gap (green long-dash). [See the electronic edition of the Journal for a color version of this figure.]

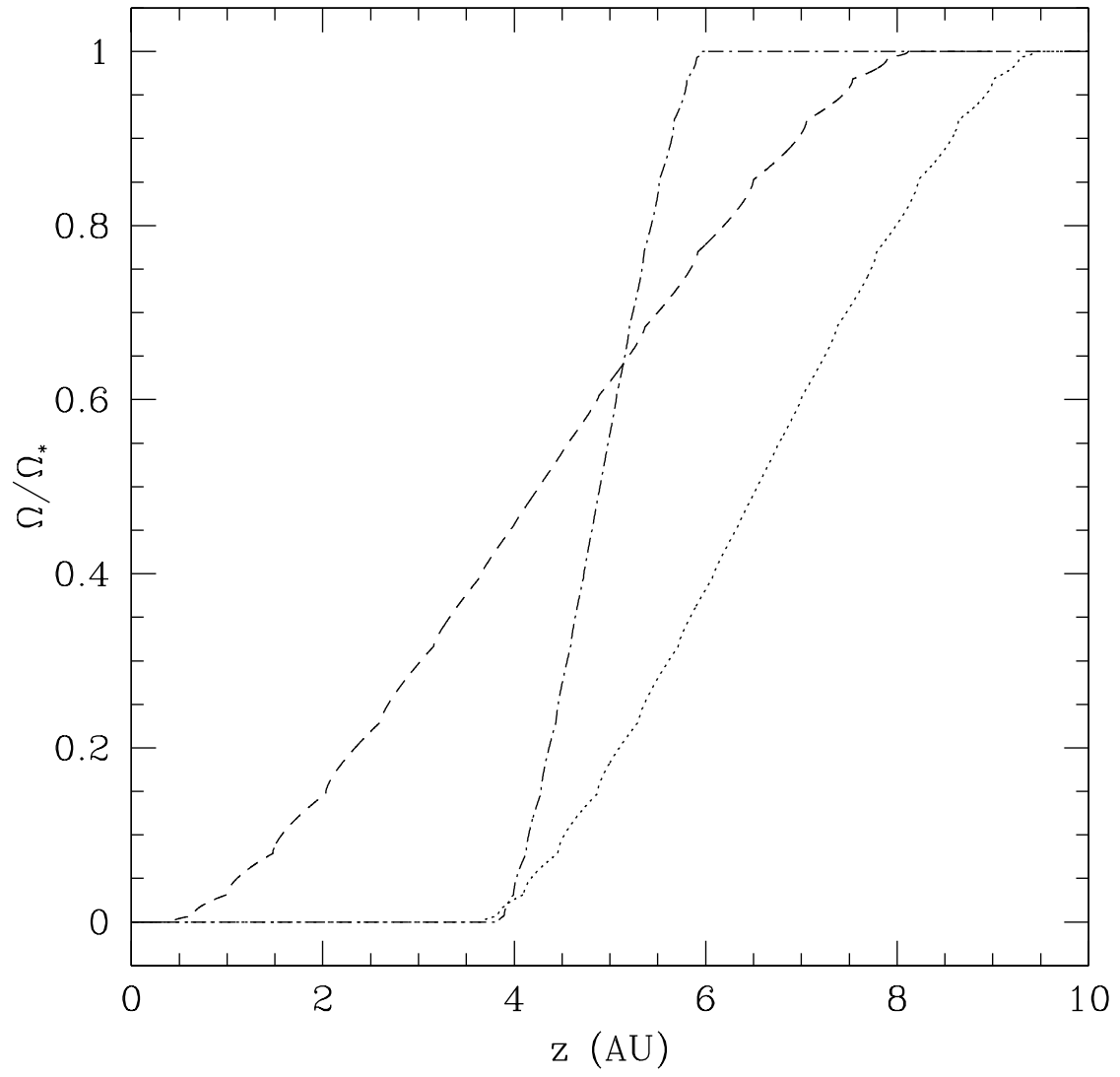


Figure 8. Solid angle of LkCa 15 (dotted line), UX Tau A (dashed line), and Rox 44 (dot-dashed line) as seen from different heights (z) at the radius of the outer wall. Ω is given in units of Ω_* , the solid angle of the entire star.

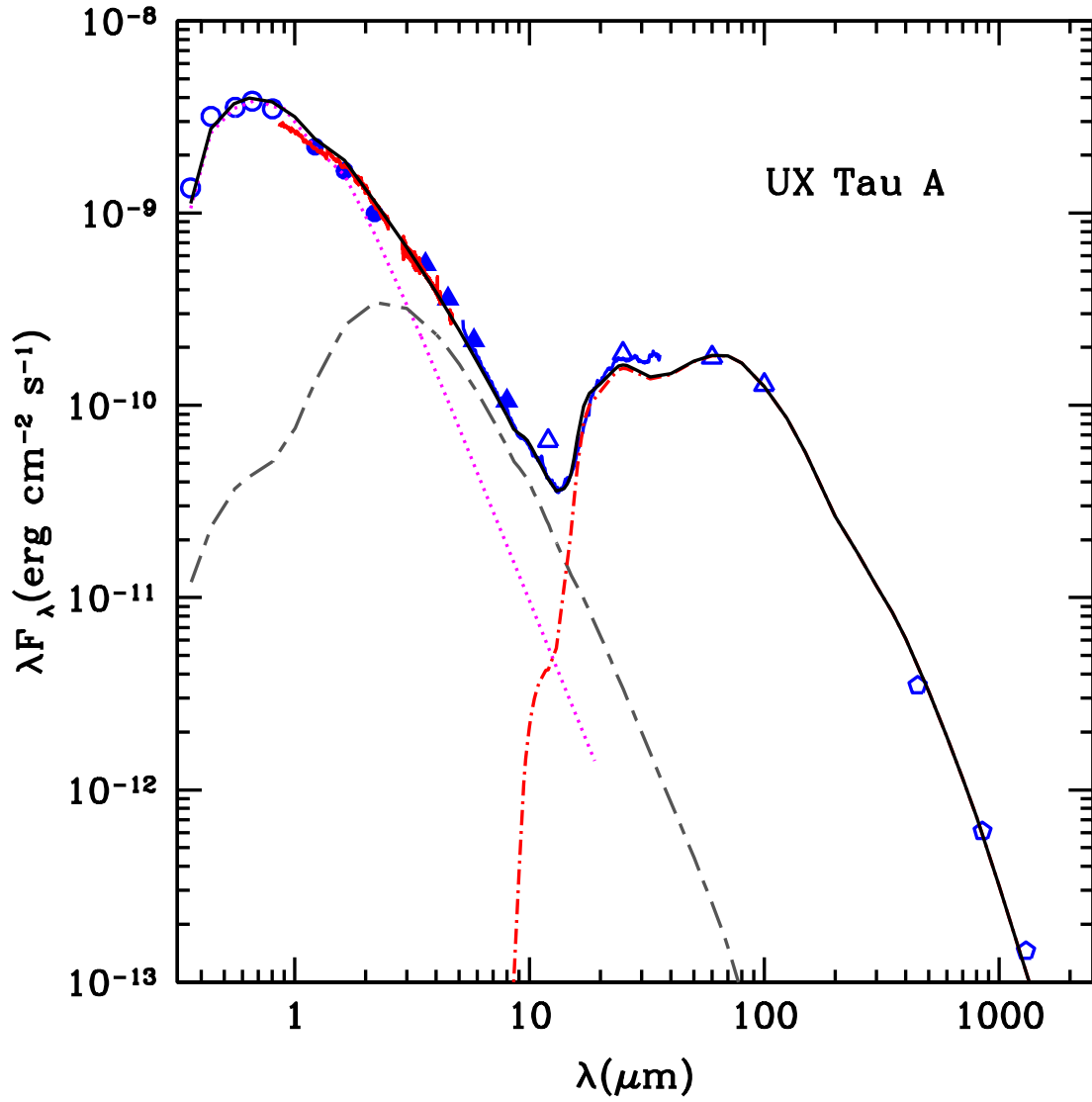


Figure 9. Pre-transitional disk model of UX Tau A. UX Tau A's best-fitting model (solid black line) has an inner optically thick disk which extends from the dust destruction radius to <0.21 AU and an outer disk from 71 – 300 AU. The gap between the inner and outer disk is relatively empty of small dust grains. Separate model components are the same as used in Figure 7. [See the electronic edition of the Journal for a color version of this figure.]

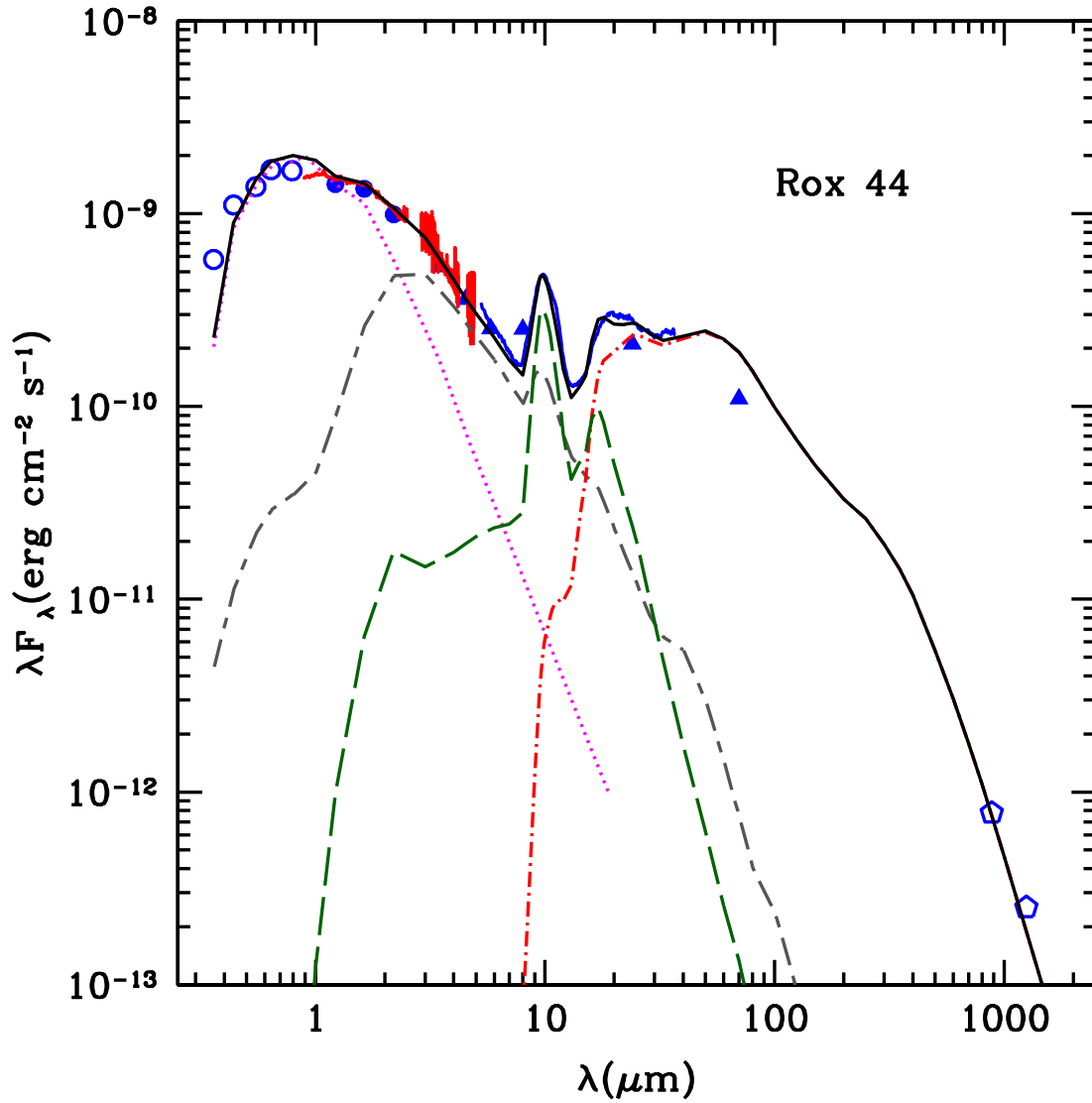


Figure 10. Pre-transitional disk model of Rox 44. The best-fit model to Rox 44 (solid black line) consists of an inner optically thick disk which extends from the dust destruction radius to <0.4 AU and an outer disk from 36 – 300 AU. Within the inner 2 AU of the gap between the inner and outer disk, there is $\sim 10^{-11} M_{\odot}$ of ISM-sized optically thin dust. Separate model components are the same as used in Figure 7. [See the electronic edition of the Journal for a color version of this figure.]

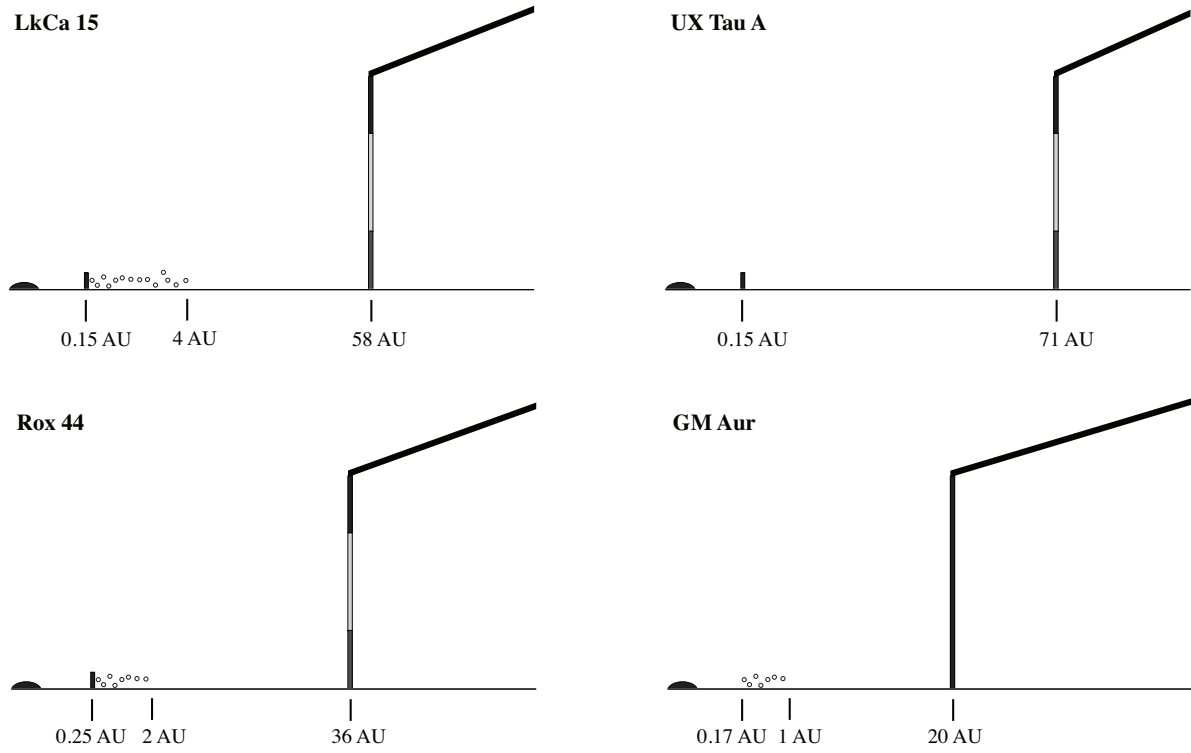


Figure 11. Schematic illustration of the pre-transitional disks of LkCa 15, UX Tau A, and Rox 44 and the transitional disk of GM Aur. The black semicircles represent the central stars and the small, empty circles are ISM-sized optically thin dust. The vertical lines are the disk walls. For the wall of the outer disk, black represents the portion of the wall that is fully illuminated by the star, light gray corresponds to the part of the wall that is in the penumbra of the inner disk, and dark gray is the portion of the wall that is in the umbra. In each case, the surface of the outer disk is fully illuminated. The transitional disk of DM Tau, which is not shown here, has an inner disk hole similar to what is seen in GM Aur, but it is devoid of optically thin small dust. Structures here are not drawn to scale.

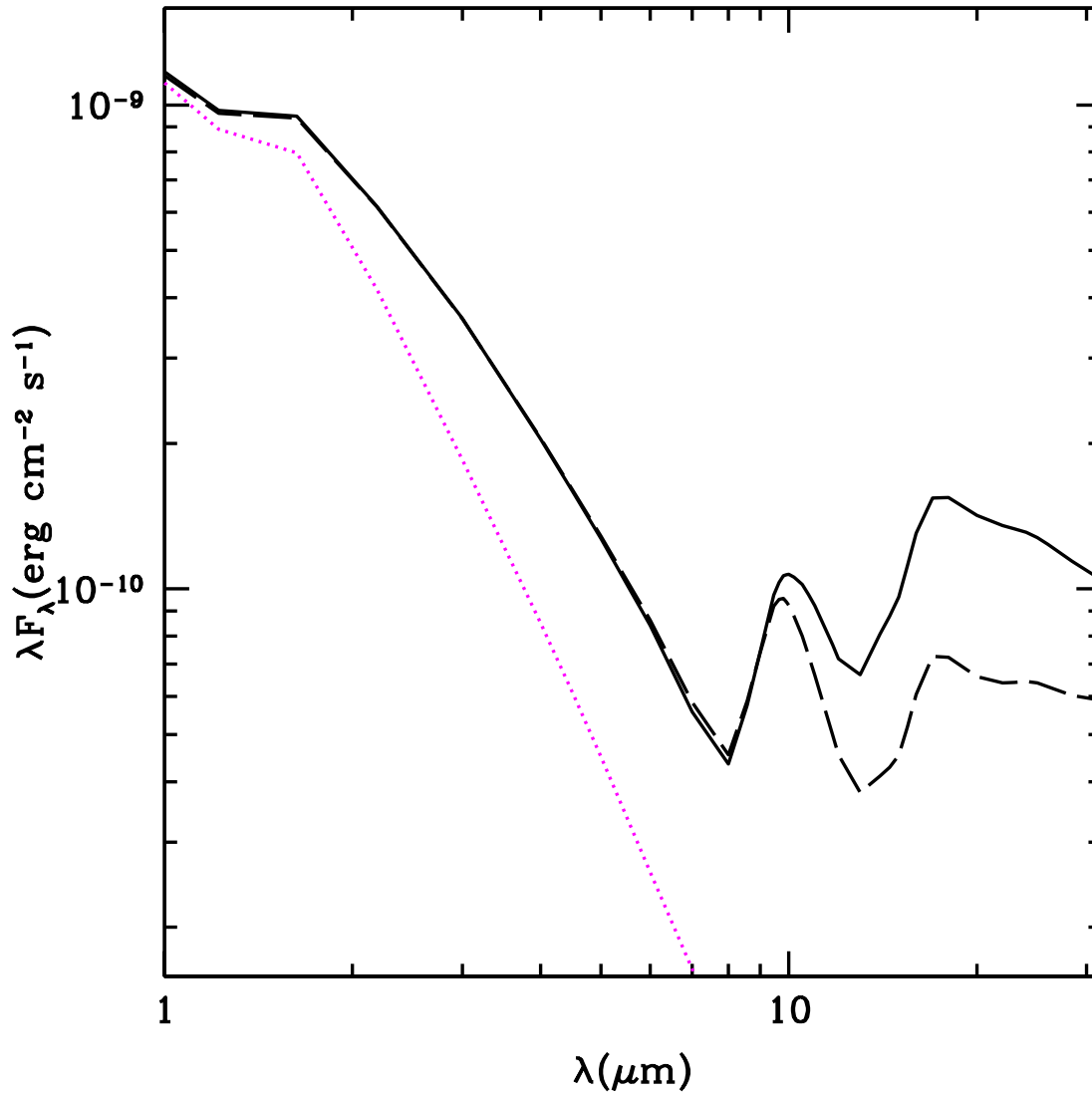


Figure 12. Simulation of a gapped disk compared to a typical full disk model. A pre-transitional disk with a gap extending from ~ 0.3 AU to 4 AU (solid line) has a SED that diverges from a full disk SED (dashed line) beyond $10 \mu\text{m}$. This is due to the contribution of the illuminated portion of the outer wall in the gapped disk model. The dotted line corresponds to the stellar photosphere.

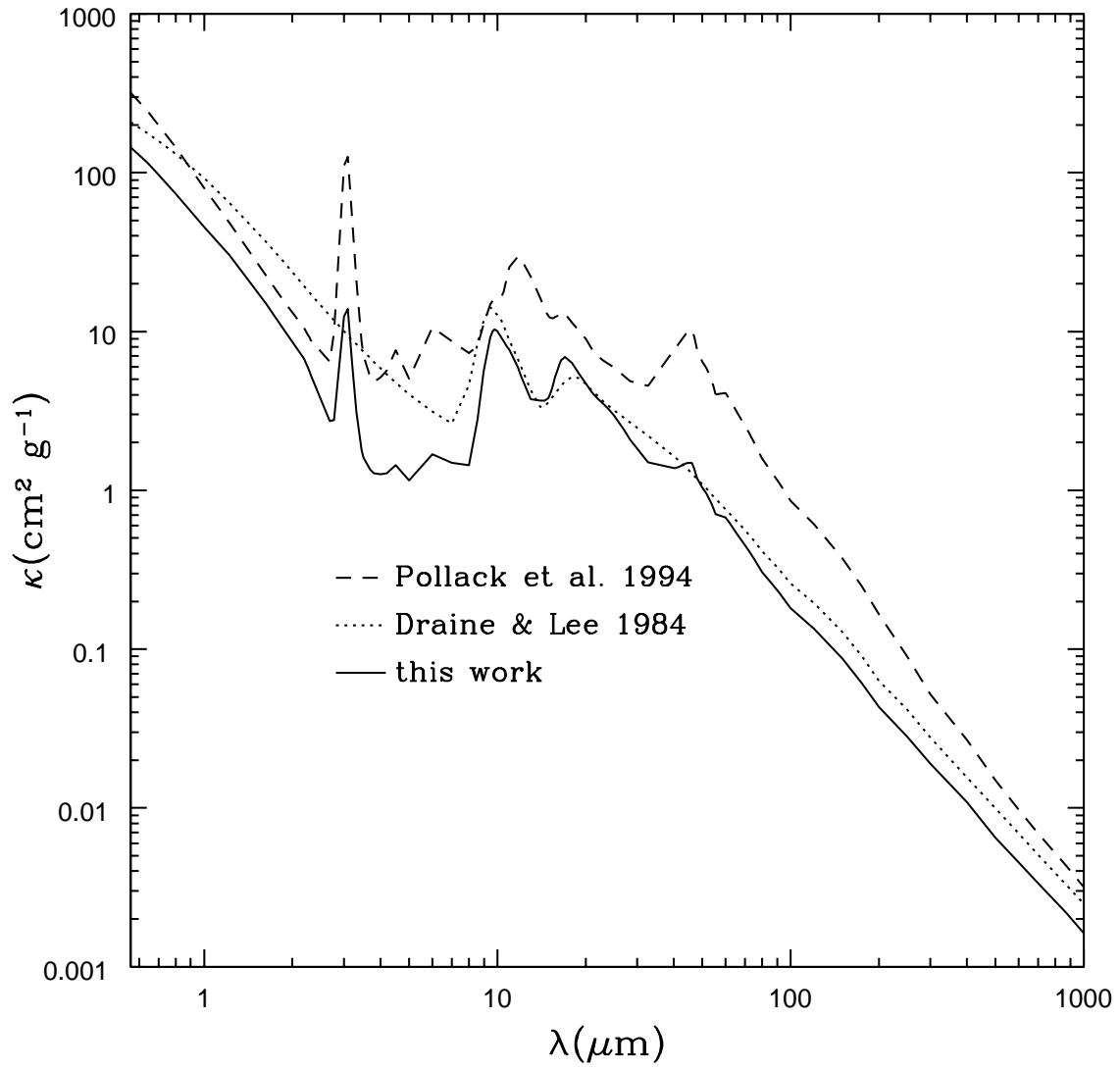


Figure 13. Comparison of the opacities adopted in this work to those from Pollack et al. (1994) and Draine & Lee (1984).

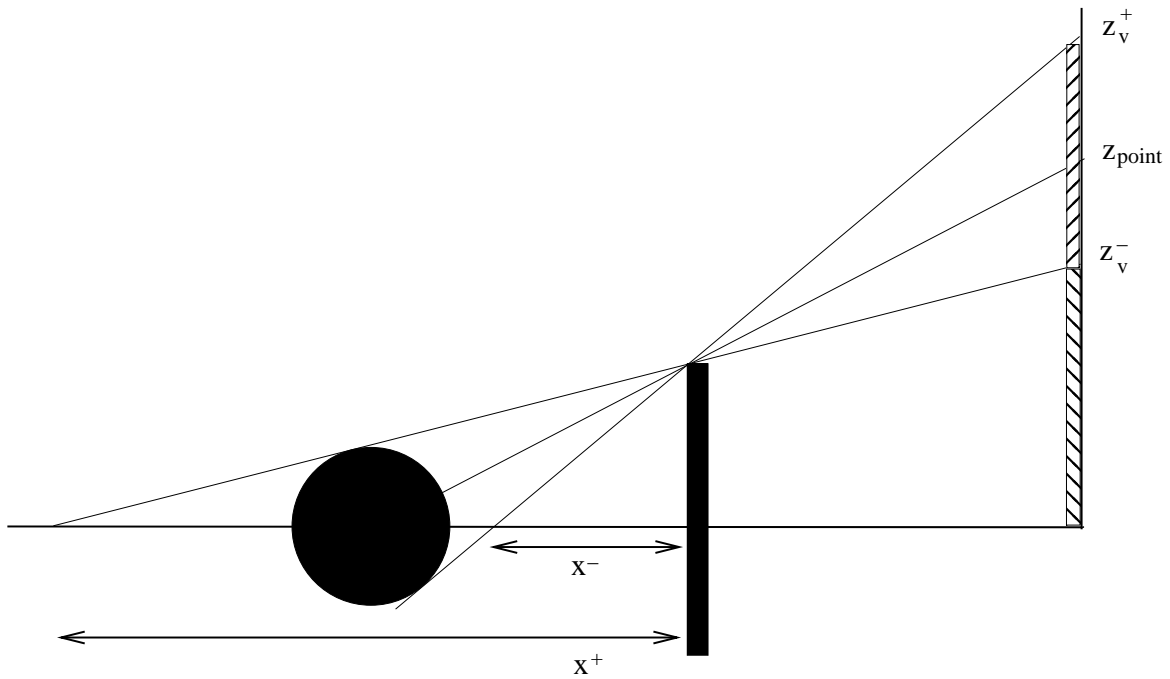


Figure 14. Limits of the shadow cast by a finite source. Above z_v^+ the whole star is visible and below z_v^- the star is in the umbra. In the intermediate region, the surface of the star is partially visible (i.e. the wall is in the penumbra). z_{point} is the height of the umbra when the star is taken to be a point source.

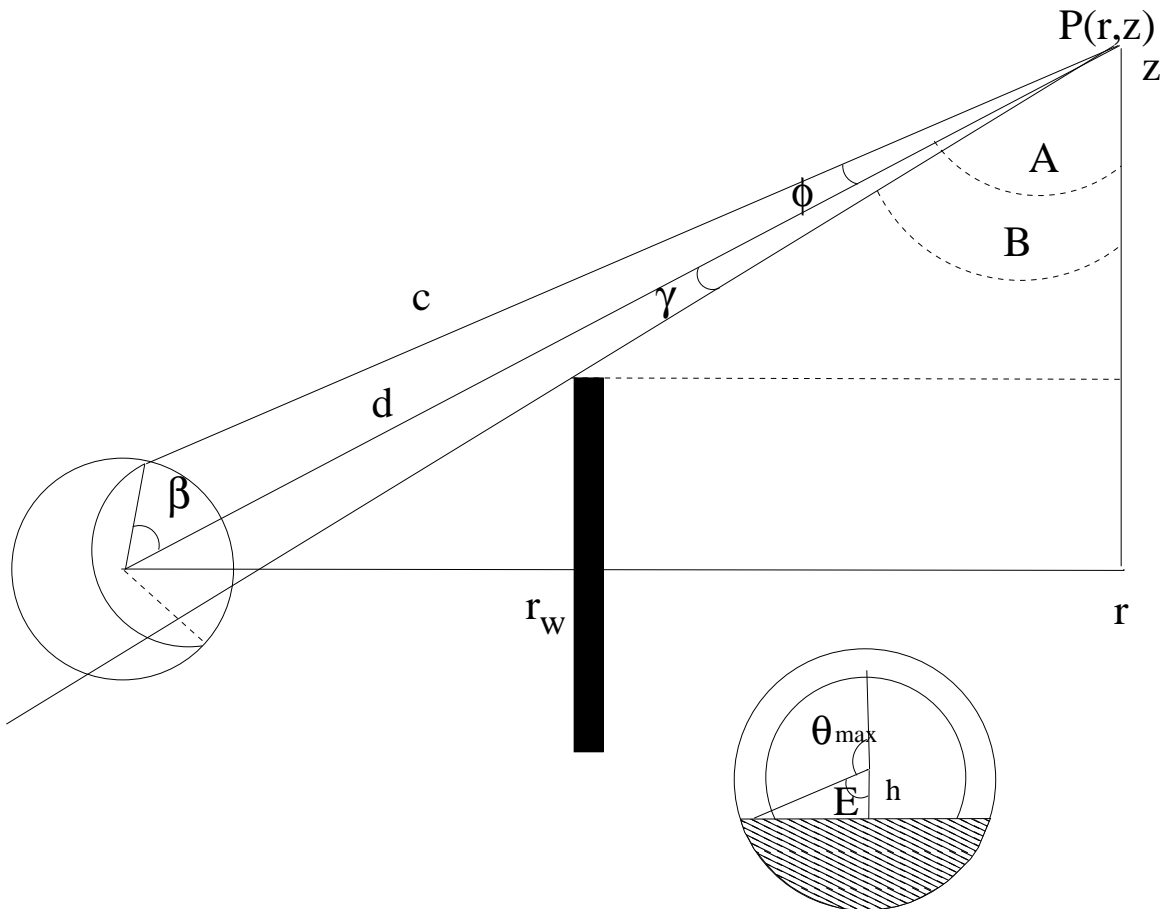


Figure 15. Geometry of the star, inner wall, and outer wall used to define the integration limits of the solid angle subtended by the star.